Quantifying sources of Brazil's CH_4 emissions between 2010 and 2018 from satellite data

Rachel L. Tunnicliffe[1,2], Anita L. Ganesan[1], Robert J. Parker[3,4], Hartmut Boesch[3,4], Nicola Gedney[5], Benjamin Poulter[6], Zhen Zhang[7], Jošt V. Lavrič[8], David Walter[8,9], Matthew Rigby[2], Stephan Henne[10], Dickon Young[2], and Simon O'Doherty[2]

[1]School of Geographical Sciences, University of Bristol, Bristol, UK
[2]School of Chemistry, University of Bristol, Bristol, UK
[3]National Centre for Earth Observation, University of Leicester, Leicester, UK
[4]Earth Observation Science, School of Physics and Astronomy, University of Leicester, Leicester, UK
[5]Met Office Hadley Centre, Joint Centre for Hydrometeorological Research, Exeter, UK
[6]NASA Goddard Space Flight Center, Biospheric Sciences Laboratory, Greenbelt, USA
[7]Department of Geographical Sciences, University of Maryland, College Park, USA
[8]Max Planck Institute for Biogeochemistry, Jena, Germany
[9]Max Planck Institute for Chemistry, Mainz, Germany
[10]Empa, Swiss Federal Laboratories for Materials Science and Technology, Dübendorf, Switzerland

Correspondence: Rachel Tunnicliffe (rachel.tunnicliffe@bristol.ac.uk)

Abstract. Brazil's CH_4 emissions over the period 2010–2018 were derived for the three main sectors of activity: anthropogenic, wetland and biomass burning. Our inverse modelling estimates were derived from GOSAT satellite measurements of XCH_4 combined with surface data from Ragged Point, Barbados and the high-resolution regional atmospheric transport model NAME. We find that Brazil's mean emissions over 2010–2018 are $33.6 \pm 3.6\,\mathrm{Tg\,yr^{-1}}$, which are comprised of $19.0 \pm 2.6\,\mathrm{Tg\,yr^{-1}}$ from anthropogenic (primarily related to agriculture and waste), $13.0 \pm 1.9\,\mathrm{Tg\,yr^{-1}}$ from wetlands and $1.7 \pm 0.3\,\mathrm{Tg\,yr^{-1}}$ from biomass burning sources. In addition, between the 2011–2013 and 2014–2018 periods, Brazil's mean emissions rose by $6.9 \pm 5.3\,\mathrm{Tg\,yr^{-1}}$ and this increase may have contributed to the accelerated global methane growth rate observed during the latter period. We find that wetland emissions from the Western Amazon increased during the start of the 2015–16 El Niño by $3.7 \pm 2.7\,\mathrm{Tg\,yr^{-1}}$ and this is likely driven by increased surface temperatures. We also find that our estimates of anthropogenic emissions are consistent with those reported by Brazil to the United Framework Convention on Climate Change. We show that satellite data is beneficial for constraining national-scale CH_4 emissions, and, through a series of sensitivity studies and validation experiments using data not assimilated in the inversion, we demonstrate that (a) calibrated ground-based data are important to include alongside satellite data in a regional inversion, and that (b) inversions must account for any offsets between the two data streams and their representations by models.

1 Introduction

Methane (CH_4) is the second most important anthropogenic greenhouse gas behind carbon dioxide due to its radiative properties and atmospheric abundance (Ciais et al., 2013). After a brief plateau period around the turn of the century (Cunnold, 2002; Dlugokencky et al., 2003), CH_4 mole fractions began rising again globally after 2007 (Rigby et al., 2008; Dlugokencky et al., 2009; Frankenberg et al., 2011; Nisbet et al., 2016) with some of the strongest growth rates occurring from 2014 onward (Nisbet et al., 2019). This increase in CH_4 growth rate was accompanied by a shift in the δ^{13}C-CH_4 isotopic ratios to more negative values, suggesting a change in the global makeup of sources and/or sinks. The drivers responsible for this shift are presently not well-understood, and proposals include increases from tropical wetlands or agriculture, decreases in biomass burning, changes in fossil fuel emissions or in the hydroxyl radical sink (e.g. Monteil et al. 2011; Schaefer et al. 2016; Schwietzke et al. 2016; Nisbet et al. 2016; Rigby et al. 2017; Worden et al. 2017; McNorton et al. 2018; Turner et al. 2019; Nisbet et al. 2019). Quantifying the CH_4 budget and understanding how major sources and sinks have evolved is key to designing emission pathways that limit global warming due to the importance of CH_4 in meeting global climate targets (Ganesan et al., 2019; Nisbet et al., 2019, 2020).

The Paris Agreement pledges to limit warming to less than 2°C with an aspiration for less than 1.5°C warming from pre-industrial levels (UNFCCC, 2015). The mitigation action taken by each country is dependent on their own Nationally Determined Contributions and accounting for national emissions will occur through inventory or "bottom-up" methods. To assess whether these self-determined targets are being met, independent estimates can be derived using "top-down" strategies that use atmospheric measurements to quantify sector-level emissions estimates at near real-time and at high-resolution (e.g. Ganesan et al., 2019). Using both top-down and bottom-up methods together for national-scale greenhouse gas estimation is considered to be best practice (Calvo Buendia et al., 2019) and allows for the greatest process-level understanding of changes in the atmosphere.

Brazil is thought to be a major contributor to global CH_4 emissions due to its variety of natural and human-made sources. Anthropogenic emissions arise from agriculture, waste and biomass burning (Ministry of Foreign Affairs et al., 2019). Brazil's 2018 Biennial Update Report to the United Framework Convention on Climate Change (UNFCCC) states that $17.6 \pm 4.0\,\mathrm{Tg}$ of CH_4 was emitted from anthropogenic sources in 2015. The majority of these emissions were from agricultural processes (70% from enteric fermentation, manure management and crop residue burning) with the remainder coming from waste (16%), energy (4%) and land-use change (6%) (Ministry of Foreign Affairs et al., 2019).

Around 60% of the Amazon basin and 80% of the Pantanal wetland region (Ministry of Science and Innovation, 2016; Schulz et al., 2019) exist within Brazil in the northern and central-western regions of the country, respectively. The primary areas of agricultural activity are in central and southern provinces and include cattle ranching and sugar cane production, while waste and fossil fuel emissions are focused in population centres along the eastern coast (Ministry of Foreign Affairs et al., 2019). Biomass burning occurs along the 'arc of deforestation' along the southern edge of the Amazon rain forest during and after the dry season (Jul-Oct). This is in contrast to Amazon wetland emissions which peak during and after the wet season (Dec-Mar).

Current top-down estimates of CH_4 emissions from Brazil, the Amazon and tropical South America vary depending on the method, source of data and area considered. In the synthesis of Saunois et al. (2016), across the Tropical South America region, emission estimates derived using different datasets and top-down methods span the large range of 63–119 $\mathrm{Tg\,yr^{-1}}$ (23–69 $\mathrm{Tg\,yr^{-1}}$ from wetlands) for 2012. Across the Amazon basin, estimates of total emissions derived from aircraft measurements are between $\sim 16-72\,\mathrm{Tg\,yr^{-1}}$ derived for May, 2009 (Beck et al., 2013) and 31–43 $\mathrm{Tg\,yr^{-1}}$ for 2010–2013 (Wilson et al., 2016; Pangala et al., 2017). A recent study that performed a regional analysis using satellite data by Janardanan et al. (2020) found Brazil's emissions alone, on average, to be $56.2\,\mathrm{Tg\,yr^{-1}}$ ($39.8 \pm 12.4\,\mathrm{Tg\,yr^{-1}}$ from wetlands) across 2011–2017. In addition, many previous studies have estimated emissions globally using satellite data (e.g., Bergamaschi et al. 2009; Feng et al. 2017). The wide range of estimates indicate that large uncertainties exist and these uncertainties are exacerbated when estimating emissions over smaller scales such as the Amazon basin or when quantifying individual sources.

Through use of a high-resolution regional inversion framework coupled with satellite measurements of CH_4, we inferred spatial and temporal distributions of Brazil's CH_4 emissions from 2010–2018. The regional inversion approach provides the benefit that uncertainties in the hydroxyl radical CH_4 sink (Rigby et al., 2017; Turner et al., 2017; Nguyen et al., 2020), a limitation in global approaches, can be neglected. Owing to a spatial and temporal difference in Brazil's major CH_4 sources, these emissions are further partitioned into source sectors (Section 3.1) and are also presented for different wetland regions (Section 3.2). We demonstrate the importance of the inversion setup when using satellite data to estimate country and basin-scale emissions. Independent validation using *in-situ* data is shown in Section 3.3 and sensitivity studies, testing a range of different input factors, are discussed in Section 3.4.

2 Methods

2.1 CH_4 measurements

We used data from three sources: (1) University of Leicester v7.2 total column CH_4 product from the Thermal And Near-infrared Sensor for carbon Observation Fourier Transform Spectrometer (TANSO-FTS) instrument on board the Greenhouse gases Observing SATellite (GOSAT) from April 2010 - Nov 2018, (2) surface data from Ragged Point, Barbados (RPB, $+13.17°$N, $-59.43°$E), and (3) surface data from the Amazon Tall Tower Observatory (ATTO, $-2.15°$N, $-59.01°$E) for external validation of the inversion. Figure 1 shows the positions of GOSAT points for a one year period and the locations of the two surface stations.

Dry-air column-averaged CH_4 mole fractions (XCH_4) were derived using the CO_2 proxy method, which multiplies the XCH_4/XCO_2 ratio by a model XCO_2 field (Parker et al., 2011, 2015). The model XCO_2 is based on the median of three global models which all assimilated surface site measurement data: GEOS-Chem (Feng et al., 2011), Carbon Tracker (Peters et al., 2007) and LMDZ (MACC/CAMS) (Chevallier et al., 2010). This GOSAT product was previously compared to aircraft measurements over the Amazon basin by extrapolating the aircraft profiles through the troposphere and using a stratospheric model, and showed differences that ranged from -1.9–$9.7\,\mathrm{nmol\,mol^{-1}}$ (Webb et al., 2016).

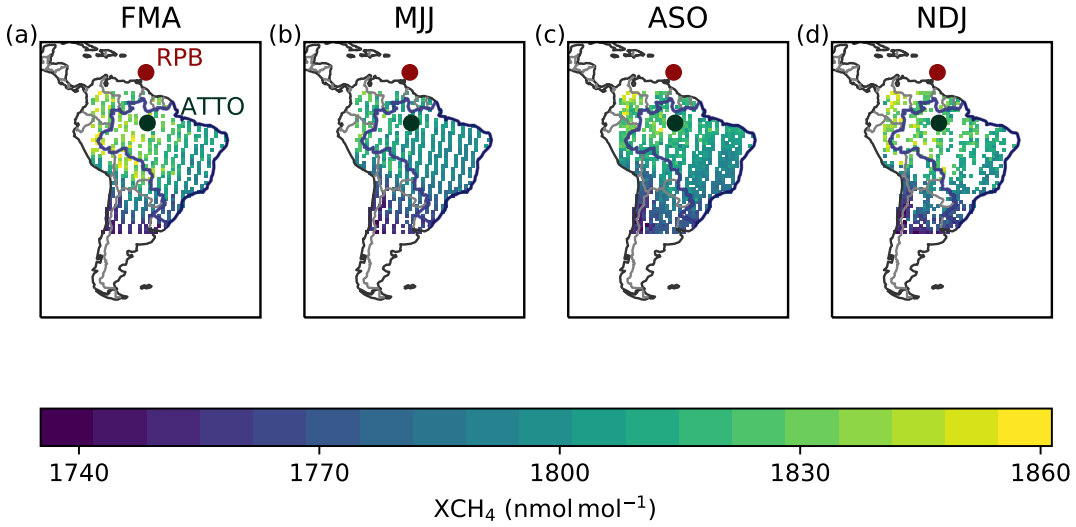

Figure 1. GOSAT measurements grouped into February-April (FMA), May-July (MJJ), August-October (ASO) and November-January (NDJ). Measurements are shown here for the 02/2014–01/2015 period and averaged in 1° bins for clarity. FMA and ASO are representative of the wet and dry seasons over the Amazon, respectively. Positions for the ATTO and RPB sites are also shown. The Brazilian border is highlighted in blue.

We used Level 2 GOSAT measurements that were taken in nadir mode within an area that extended from -35.8 to $7.3°$N and -76.0 to $-32.8°$E and that passed the quality threshold. We only used nadir measurements to minimise the effect of any unquantified biases between nadir and glint mode. In addition, we filtered data where the surface pressure deviated from the retrieval grid by enough to reduce the number of retrieval levels to less than 20. The remaining data points were averaged across a $0.23 \times 0.35°$ grid to match the lowest resolution of the atmospheric transport model grid cell (see section 2.3) across the 2010–2018 time period leaving ~ 1300 data points on average per month.

Data from RPB were used alongside the satellite measurements in the inversion to provide additional constraints on the boundary conditions. RPB is part of the Advanced Global Atmospheric Gases Experiment (AGAGE) network (Prinn et al., 2018) and predominantly measures well-mixed background air. Measurements up to 2017 were made using GC-FID (Gas Chromatography Flame - Ionization Detector) and beyond this with a CRDS (Cavity Ring-down Spectrometer) instrument. All data were averaged into hourly samples.

Measurements from ATTO (Andreae et al., 2015; Botía B. et al., 2019) were used for external validation of the inversion results. ATTO is located near Manaus within the Amazon rainforest. The position and predominant north-easterly wind direction means that this site is particularly sensitive to CH_4 emitted from wetlands but may also receive air masses from regions of biomass burning and other human activity (Andreae et al., 2015; Pöhlker et al., 2019). CH_4 mole fractions from 2014–2018

derived from CRDS instrumentation have been used in this study. Hourly mean measurements from the highest inlet on the tower, at 79 m, were used as they are assumed to be the most representative of regional air masses.

2.2 Atmospheric Transport Model

To provide the relationship between atmospheric mole fractions at a receptor and a surface emissions field, we used the high-resolution Lagrangian atmospheric transport model NAME (Numerical Atmospheric dispersion Modelling Environment) (Jones et al., 2007). Model particles were released for each GOSAT and surface measurement time and location and tracked backward in time for 30 days. The model tracked the interaction of these particles with the surface (defined as 0–40 m above modelled ground level) to quantify the sensitivity to regional emissions. The times and locations that particles left the model domain was recorded to quantify the sensitivity to boundary conditions. NAME was driven by meteorological inputs from the Unified Model (UM) spanning resolutions between 0.23 to 0.09° latitude and 0.35 to 0.14° longitude over the 2010–2018 period. The annual mean sensitivity to GOSAT measurements used in this study are shown in Appendix Fig. A1.

Satellite measurements require footprints of the total atmospheric column and model particles were released at multiple heights based on the pressure levels defined within the GOSAT product (see Ganesan et al. 2017 for a description of how NAME was used to simulate XCH_4 by applying averaging kernels, pressure weights and *a priori* information for satellite data). The main modification in the NAME setup from Ganesan et al. (2017) made here is that surface pressure in GOSAT was corrected to match the surface pressure from the UM. Occasionally, the corrected surface pressure level was lower than the first model level, and in these cases, the retrievals were discarded. This ensured consistency between the model defining the GOSAT pressure levels and NAME.

2.3 Inversion method

Top-down emissions estimates were inferred using a hierarchical Bayesian inversion method with reversible jump, trans-dimensional Markov chain Monte Carlo (MCMC). A full description of the method can be found in Ganesan et al. (2014) and Lunt et al. (2016). The hierarchical component employs a set of hyperparameters that define the model-measurement and prior emissions uncertainties, and which were explored as part of the inversion. Inclusion of these additional model parameters allows for uncertainties in the system to be more accurately captured. The trans-dimensional component of the inversion allowed for the spatial inversion grid to be estimated as part of the inversion, rather than being defined *a priori*.

The *a priori* inputs to the inversion are described in Section 2.4. The emissions PDF was defined as lognormal to prevent non-physical negative solutions from being reached. The standard deviation of this PDF was allowed to vary between 0.05 and 20.0 (with a value of one being equivalent to the prior emissions magnitude). The model-measurement uncertainty, was governed by a Gaussian distribution centred on zero with a standard deviation that was a hyper-parameter in the inversion. The standard deviation hyper-parameter was described by a uniform distribution with a range of 0.2 to 200 $\mathrm{nmol\,mol^{-1}}$.

Each month, we estimated emissions from within the NAME domain (at the resolution explored by the trans-dimensional method), as well as offsets to *a priori* boundary condition "curtains" on each edge of the domain (Section 2.4). In addition, an offset parameter was included to account for any differences between the satellite and the calibrated ground-based measure-

ments and their representation by models. A normal PDF was defined for both of these types of offsets, centred around zero, and where the standard deviation of the PDFs were governed by hyper-parameters. The standard deviations of the boundary condition offsets were allowed to vary up to $100.0\,\mathrm{nmol\,mol^{-1}}$ and up to $50.0\,\mathrm{nmol\,mol^{-1}}$ for the offset between surface and satellite data. The necessity of this parameter to produce the most robust results is discussed in Section 3.3.

The Metropolis-Hastings MCMC sampler was run with $500,000$ iterations with the initial $100,000$ samples discarded as burn-in. Every 500^{th} iteration was saved and used to build posterior PDFs for each parameter. The mean and 2.5–97.5 percentiles were used to produce posterior estimates and 95% confidence intervals.

2.4 *A priori* fields

A priori emissions and boundary condition fields are summarised in Table 1. Emissions were inferred for the three major source sectors in Brazil: anthropogenic, biomass burning and wetlands. Maps for two representative months in the wet (January) and dry (September) seasons for 2014 are shown for each sector in Fig. 2.

Anthropogenic emissions, excluding biomass burning, were from the EDGAR (Emission Database for Global Atmospheric Research) v4.3.2 database (Janssens-Maenhout et al., 2017). Annual emissions were available up to 2012 and then assumed to be equal to the 2012 emissions thereafter. The biomass burning contribution was from GFED (Global Fire Emissions Database) v4.1 (Van Der Werf et al., 2017) at monthly resolution to the year 2015 and assumed to be held at 2015 values thereafter.

Wetland emissions were based on the output from the JULES land surface model (Clark et al., 2011) which was modified to use the wetland fractional map from Surface WAter Microwave Product Series (SWAMPS). We used a version of SWAMPS that was updated from Schroeder et al. (2015) to include wetlands occurring under dense canopies, to remove rice agriculture and to include any inland water. Wetland emissions across South America were scaled to $44\,\mathrm{Tg\,yr^{-1}}$ based on the mean bottom-up estimate for Tropical South America from Saunois et al. (2016).

A priori mole fractions at the boundaries of the domain were derived from the CAMS CH_4 flux inversion product v17r1 (accessible at https://apps.ecmwf.int/datasets/data/cams-ghg-inversions/). This version assimilated the global surface measurement network and did not use satellite data. This product was only available up to 2017, so to extend the analysis to 2018, the climatological mean of the 2010–2017 period was used.

2.5 Sector attribution

The total emissions estimated from the inversion were partitioned into each of the three major source sectors using the fraction of each source in the *a priori* emission fields in each grid cell. Due to the largely distinct spatial or temporal distributions of the sectors as shown in Fig. 3, the fractional map of each source is not overly dependent on the inventories used. The influence of the *a priori* distributions on the robustness of the sector partitioning is discussed in Section 3.4.

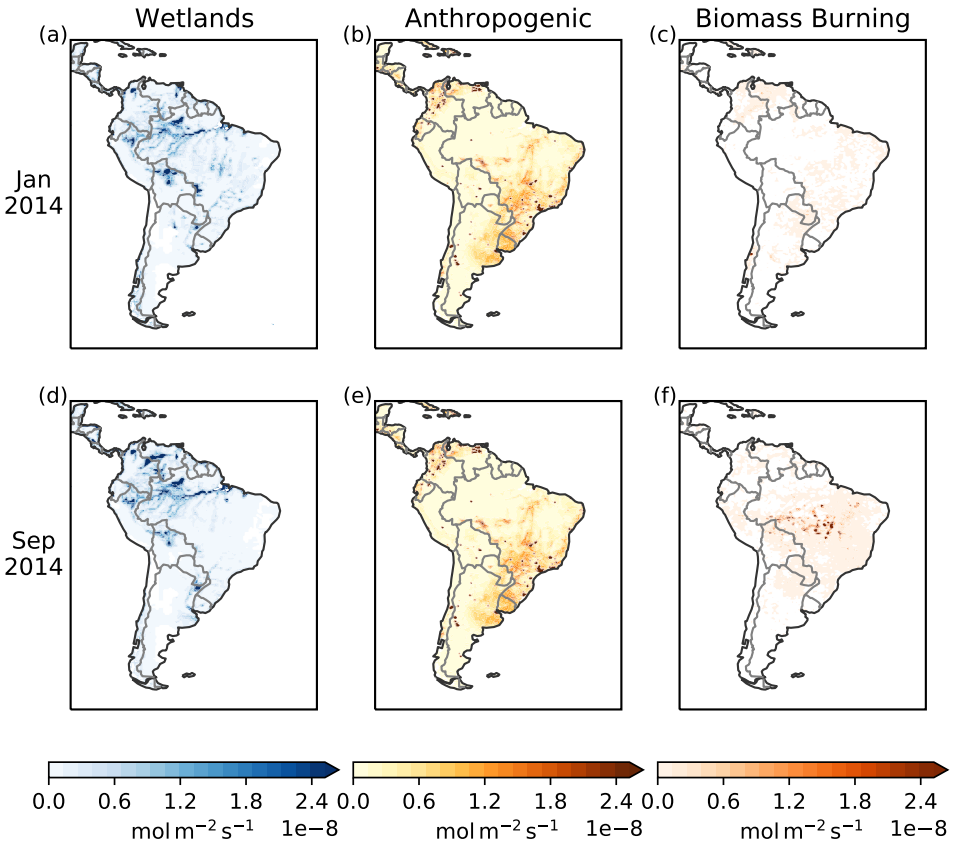

Figure 2. *A priori* emissions for wetlands, anthropogenic and biomass burning sectors for January and September, 2014. These months are representative of peak wetland extent in the wet season (January) and biomass burning activity (September). Note that the EDGAR anthropogenic inventory is annual resolution and is shown here for 2012.

2.6 Validation with ATTO

To provide a validation of the inversion results, we compared a model prediction of mole fractions at ATTO derived from hourly NAME sensitivities convolved with our posterior emissions maps and boundary conditions against measured values. Four tests were run using different configurations of the inversion. The first three estimates were from inversions that used variants of the GOSAT and RPB dataset. The first inversion utilised GOSAT data alone. The second inversion used both GOSAT and RPB measurements but did not include an offset parameter between satellite and surface data in the inversion. The third inversion used GOSAT and RPB measurements and included an offset parameter that was estimated in the inversion (our main results). These tests and the resulting comparisons with ATTO data allowed us to determine the factors that are most important when using satellite data to constrain country-scale emissions. We performed a final test which scaled our posterior emissions map so

Table 1. Summary of *a priori* emissions and boundary conditions used in this study. All maps have been re-gridded to 0.23° latitude by 0.35° longitude resolution. * Repeats this year thereafter. † For 2018, a climatological mean of 2011–2017 period was used.

Field	Source	Resolution	Time Period	Modifications
Anthropogenic emissions	EDGAR v4.3.2	Annual	2010–2012*	Excluded agricultural waste burning and combustion from manufacturing, solid waste and fossil fuels.
Wetland emissions	JULES / SWAMPS	Monthly	2010–2017*	Emissions from JULES over fractional wetland extent from SWAMPS. Total wetland emissions scaled to $44\,\mathrm{Tg\,yr^{-1}}$
Biomass burning emissions	GFED v4.1	Monthly	2010–2015*	*None*
CH_4 mole fraction curtains	CAMS v17r1	Monthly	2010-2017†	*None*

that emissions from the Brazilian Amazon matched those derived by Wilson et al. (2016) using four aircraft sites. For the whole Amazon Basin, the lowest value in the range presented in Wilson et al. (2016) of $31.6\,\mathrm{Tg\,yr^{-1}}$ was used, with $\sim 19\,\mathrm{Tg\,yr^{-1}}$ coming from the Brazilian Amazon, based on wetland extent. This test allowed us to investigate the fit of previous results against ATTO data.

In addition to these experiments, we simulated the model prediction at ATTO using a second regional Lagrangian model, the FLEXible PARTicle dispersion model (FLEXPART), for 2014–2017 (Pisso et al., 2019). The setup for FLEXPART was the same as NAME, except the surface was defined as 0–$50\,\mathrm{m}$ above ground level and the meteorological drivers were 1° resolution from the European Centre for Medium-Range Weather Forecasts (ECMWF). Particles were tracked backwards for 30 days. This test allowed us to assess whether results are significantly impacted by systematic uncertainties in NAME.

2.7 Sensitivity Studies

Sensitivity tests against a range of inputs to the inversion were performed to assess the robustness of our results. Three categories of inputs were tested: *a priori* emissions, *a priori* boundary conditions and the model XCO_2 fields used to derive XCH_4. In most cases, comparisons were performed for 2014 only, but if differences were seen, the analysis was expanded across the entire time range of 2010–2018. The sensitivity study details are summarised in Table 2.

To test the sensitivity to *a priori* emissions, we ran a set of inversions where emissions were perturbed one at a time from each source sector. We changed the magnitudes of emissions from each sector and tested variations of wetland extent maps. For the latter, three additional wetland distributions were used: two using JULES emissions either with Bergamaschi et al. (2007) (hereafter referred to as Kaplan, which is based on land cover maps from optical imagery) or the high-resolution Tropical and Sub-Tropical Wetland Distribution v2.0 (Gumbricht et al. 2017, hereafter referred to as Gumbricht). The final variation used the Wetland CH_4 emission and uncertainty dataset for atmospheric chemistry and transport modelling (WetCHARTs) based on an ensemble of wetland models (Bloom et al., 2017). We did not modify these wetland distributions to include any emissions

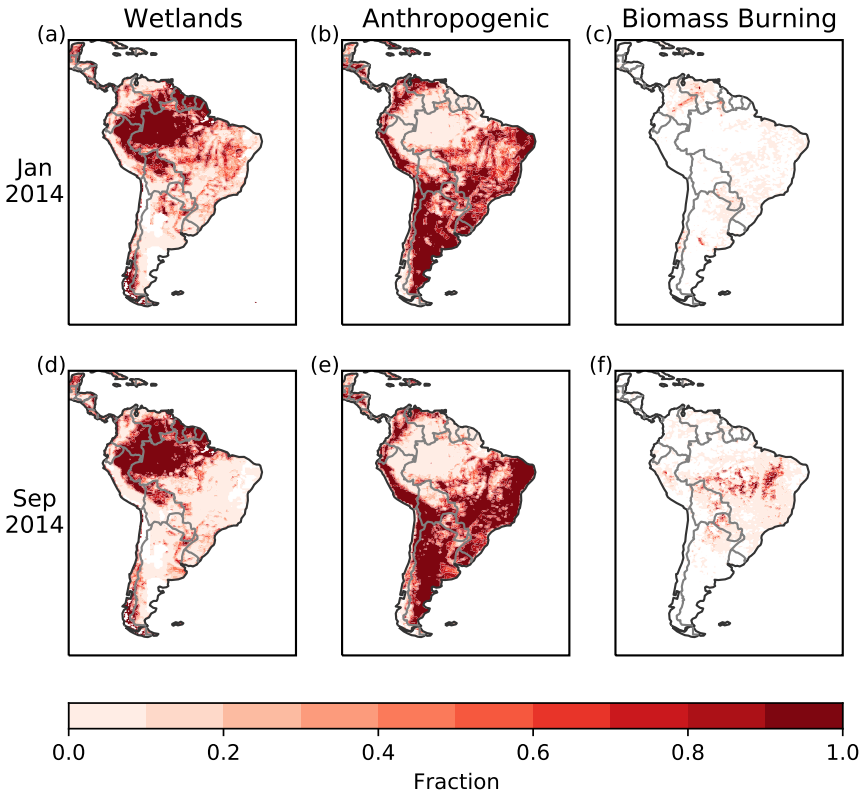

Figure 3. Fraction of wetland, anthropogenic and biomass burning emissions for January (top panel) and September (bottom panel) 2014 derived from the *a priori* emissions. Note that the EDGAR anthropogenic inventory is annual resolution and is shown here for 2012.

that might occur when the water table is below the surface. These four wetland distribution maps are shown in Appendix Fig. A2.

To test the sensitivity to *a priori* boundary conditions, we used a variation of the global mole fractions used to generate the boundary condition curtains. We used the climatological mean of the MOZART global model (Emmons et al., 2010) over 2010–2014 time period. The setup for MOZART is described in Palmer et al. (2018).

To test the sensitivity to the model XCO_2 used to derive XCH_4, we generated 10 variations of XCH_4 for each measurement. These were created by randomly selecting between the median (the main results) and the extremes in the ensemble members that are included with the data product. We re-ran the inversion for each of the ten datasets for the full 2010–2018 time period, which allowed us to investigate random errors in XCO_2. However, additional uncertainties could nevertheless remain due to sparse CO_2 observations in the region.

Table 2. Sensitivity studies performed in this study for *a priori* fields or for model XCO_2. For the *a priori* emissions, each sector was varied one at a time over the full South America domain with other sectors kept in their original configurations.
† Based on bottom-up emissions estimates from Saunois et al. (2016) for tropical South America.

Experiment category	**Experiment name**	**Description**
Wetland distribution	Kaplan	JULES emissions and wetland extent from Bergamaschi et al. (2007). Wetlands emissions scaled to $44\,\mathrm{Tg\,yr^{-1}}$.
	Gumbricht	JULES emissions and wetland extent from Gumbricht et al. (2017). Wetlands emissions scaled to $44\,\mathrm{Tg\,yr^{-1}}$.
	WetCHARTs	Wetland CH_4 emissions from WetCHARTs v1.0 (mean of extended model ensemble) (Bloom et al., 2017).
Wetland magnitude	Saunois high	Wetlands emissions (JULES emissions and SWAMPS extent) scaled to $34\,\mathrm{Tg\,yr^{-1}}$ †.
	Saunois low	Wetlands emissions (JULES emissions and SWAMPS extent) scaled to $50\,\mathrm{Tg\,yr^{-1}}$ †.
Anthropogenic magnitude	EDGAR x 2.0	Anthropogenic emissions (EDGAR v4.3.2) doubled to $77.5\,\mathrm{Tg\,yr^{-1}}$.
Biomass burning magnitude	GFED x 2.0	Monthly biomass burning emissions (GFED v4.1) doubled (monthly max. $20.9\,\mathrm{Tg\,yr^{-1}}$).
Boundary conditions	MOZART	Climatological mean of MOZART model (Emmons et al., 2010; Palmer et al., 2018).
XCO_2 variations	XCH_4 samples	10 XCH_4 datasets created by randomly selecting across the median and the extremes for the XCO_2 model ensemble, compiled of GEOS-Chem, CarbonTracker and LMDZ (MACC/CAMS).

3 Results

3.1 Annual and seasonal emissions by sector

Mean emissions from 2010–2018 for Brazil are $33.6 \pm 3.6\,\mathrm{Tg\,yr^{-1}}$ (Fig. 4). These emissions correspond to mean anthropogenic emissions of $19.0 \pm 2.6\,\mathrm{Tg\,yr^{-1}}$, mean wetland emissions of $13.0 \pm 1.9\,\mathrm{Tg\,yr^{-1}}$, and mean biomass burning emissions of $1.7 \pm 0.3\,\mathrm{Tg\,yr^{-1}}$. Maps of these posterior emissions and the difference from the *a priori* inputs are shown for each season in Appendix Fig. A3.

Both our 2012 and 2015 estimates of anthropogenic emissions of $16.2 \pm 3.0\,\mathrm{Tg\,yr^{-1}}$ and $18.3 \pm 2.5\,\mathrm{Tg\,yr^{-1}}$ are consistent within uncertainties with Brazil's Third Biennial Update Report to the UNFCCC, which estimates $15.6\,\mathrm{Tg\,yr^{-1}}$ in 2012 and $16.3 \pm 3.8\,\mathrm{Tg\,yr^{-1}}$ in 2015 (Ministry of Foreign Affairs et al., 2019), when LULUCF contributions are removed.

The overall rise in emissions over the 2010–2018 period generally occurred in late 2013 and early 2014 and was sustained thereafter. Average emissions between 2014–2018 rose over 2011–2013 levels by $6.9 \pm 5.3\,\mathrm{Tg\,yr^{-1}}$ and this is driven by changes in anthropogenic, wetland, and biomass burning emissions of $3.3 \pm 3.7\,\mathrm{Tg\,yr^{-1}}$, $2.6 \pm 2.8\,\mathrm{Tg\,yr^{-1}}$, and $1.0 \pm 0.4\,\mathrm{Tg\,yr^{-1}}$, respectively.

Across 2010–2018, we find that total emissions maximise in April and minimise in October, and the overall seasonality reflects the net effect of different seasonal patterns in the three sectors. Anthropogenic emissions, the largest sector, peak in April and are lowest in August - October (dry season), and could be a result of seasonality in cattle, manure management (e.g. Cardoso et al. 2019) or landfill emissions (e.g. Machado et al. 2009; Imbiriba et al. 2020). Anthropogenic emissions are only estimated annually in EDGAR and in reports to the UNFCCC, and thus do not capture this important feature. Wetland emissions peak during the wet season between February and April and are lowest in October and this seasonality is more pronounced in our estimates than in the *a priori* emissions. Anthropogenic and wetland emissions are discussed further for different regions of Brazil in Section 3.2. Biomass burning emissions maximise in September and the seasonality is consistent with GFED.

Our analysis shows that individual years show some differences from the bottom-up estimates. We find the largest biomass burning emissions in 2010, a year with strong drought and intensive burning due to high Atlantic sea surface temperatures (Lewis et al., 2011; van der Laan-Luijkx et al., 2015); annual mean emissions in 2010 were $5.5 \pm 0.5\,\mathrm{Tgyr^{-1}}$ (based on Apr-Dec due to availability of GOSAT measurements in 2010), but with a monthly value in September at $22.3^{+2.6}_{-2.7}\,\mathrm{Tg\,yr^{-1}}$, a value that is $6.3\,\mathrm{Tg\,yr^{-1}}$ larger than reflected in GFED. Our estimates are consistent with GFED at most other times. Wetland emissions are highest in 2015, which corresponds to a strong El Niño year. The *a priori* model emissions do not capture the increase in 2015 but do simulate a decrease from 2016. This feature is discussed further in Section 3.2.

The performance of the inversion is demonstrated through a comparison of modelled mole fractions derived from the posterior emissions and boundary conditions with the measurements used in inversion. We show this fit for both GOSAT and RPB in Appendix Fig. A4 and we find both data sets to be represented well by the inversion.

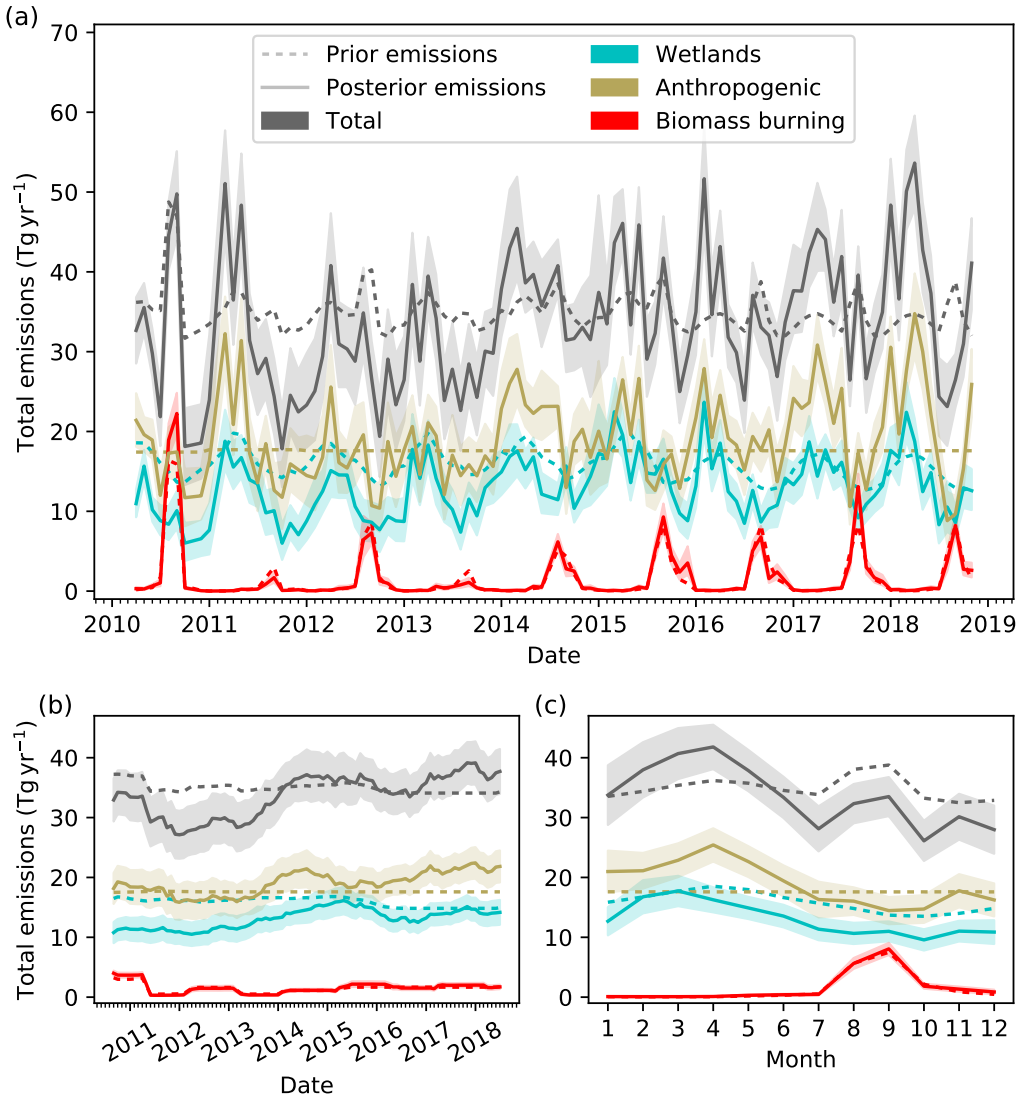

Figure 4. Brazil's CH_4 emissions derived from GOSAT and RPB measurements between 2010 and 2018. Total emissions (grey) are split into the three major sectors: wetlands (cyan), anthropogenic (yellow) and biomass burning (red). Prior and posterior emissions are dashed and solid lines, respectively. Shading indicates the 95% confidence interval. (a) Monthly emissions, (b) monthly emissions smoothed with a 12-month rolling mean and (c) monthly means across the 2010 to 2018 period. Errors in mean values assume a 50% correlation between individual months.

3.2 Sub-national emissions

In addition to the Brazilian totals presented above, we aggregated our posterior emissions for the major regions of Brazil: the Amazon basin, the Pantanal and the remainder of the country (Figs. 5 and 6 for wetland and anthropogenic sectors, respectively). The Amazon basin was defined using the TRANSCOM definition for Tropical South America (Saunois et al., 2016) and the Pantanal region was defined using the TRIP River Routing Model output (Oki et al., 1999). These regions were further masked to only include the area within Brazil using the public domain Natural Earth database (https://www.naturalearthdata.com/).

We aggregated wetland emissions (Fig. 5) into mean values for the 2010–2018 period, changes between 2011–2013 and 2014–2018, and means for each month. Mean wetland emissions from the Brazilian Amazon and Pantanal regions across the 2010–2018 period are $9.2 \pm 1.8\,\mathrm{Tg\,yr^{-1}}$ and $1.9 \pm 0.5\,\mathrm{Tg\,yr^{-1}}$, respectively. Wetland emissions in the Amazon and Pantanal comprise 65% and 26% of total emissions, respectively, with emissions from the Pantanal being dominated by the anthropogenic sector. While emissions from the Pantanal are not significantly different from the *a priori* emissions, these results are found to be robust in our sensitivity studies as discussed in Section 3.4. There is only a small change in wetland emissions over the two regions between 2011–2013 and 2014–2018. Differences are $1.5 \pm 2.6\,\mathrm{Tg\,yr^{-1}}$ and $1.0 \pm 0.7\,\mathrm{Tg\,yr^{-1}}$, for the Amazon and Pantanal, respectively. Only the small Pantanal change is significant within the 95% confidence interval. We also find that there is an offset in peak emissions between the Amazon and the Pantanal regions. Amazon wetland emissions peak around February-March whereas the Pantanal peaks in April. The seasonality for the Amazon is earlier than reflected in the *a priori* emissions.

Because wetland emissions from the Pantanal exhibit a similar seasonal pattern to the seasonality in anthropogenic emissions across Brazil, we analysed the regions that are responsible for driving the anthropogenic seasonal cycle. Figure 6 shows the anthropogenic emissions aggregated over the Amazon and Pantanal regions and over the remaining Brazilian territory. We find that the seasonal cycle is dominated by the emissions outside of the Amazon and the Pantanal. Therefore, while Pantanal wetland and anthropogenic emissions have the same seasonal pattern, this is not due to a mis-attribution between sectors based on the current configuration of the wetland and anthropogenic prior emissions. However, it is important to note the difficulty of wetland models in capturing the full seasonal cycle in the Pantanal due to overbank inundation, so there could be some uncertainty in the fractional partitioning due to uncertainty in the wetland models used in the main results and in the sensitivity studies (Parker et al., 2018).

Wetland emissions are $3.9 \pm 3.0\,\mathrm{Tg\,yr^{-1}}$ larger in the 2015 wet season relative to 2011–2014, a feature that is not present in the *a priori* emissions. We show in Fig. 7 that this increase is driven from the Amazon and not by Pantanal wetlands. We investigated changes in some of the major environmental influences to understand what could drive this pattern. Figure 7 shows our derived emission maps, changes in surface temperature from the WFDEI meteorological dataset (https://rda.ucar.edu/datasets/ds314.2/) and changes in SWAMPS inundation for the wet season, defined as February–April (FMA). We show differences between 2015 and 2011–2014 and between 2016 and 2015 for the Amazon and the Pantanal regions.

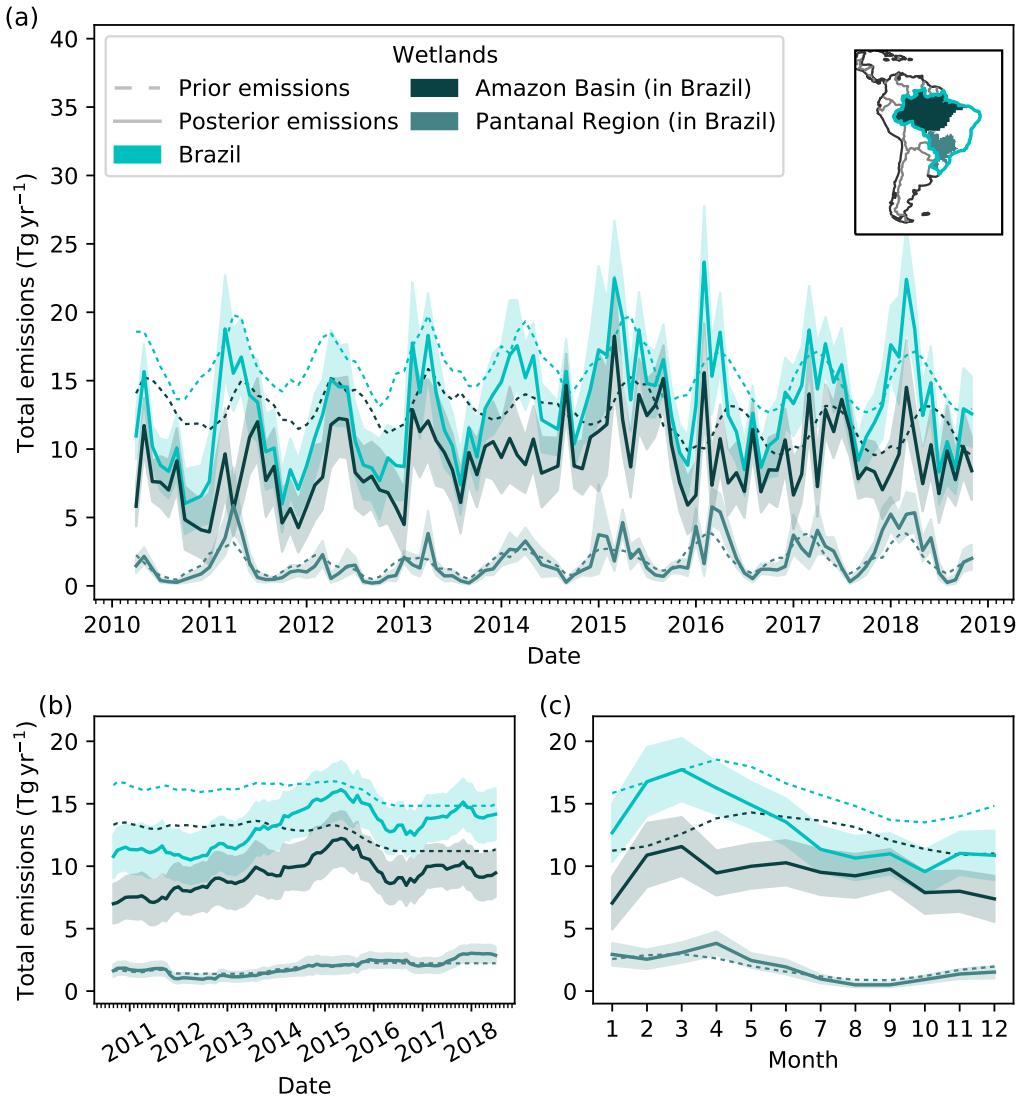

Figure 5. Brazil's wetland emissions aggregated over Amazon and Pantanal regions. (a) Monthly emissions with an inset map showing the masks used to delineate between the Amazon and Pantanal regions, (b) monthly emissions smoothed with a 12-month rolling mean and (c) seasonal means across the 2010 to 2018 period. Errors for mean values assume a 50% correlation between individual months.

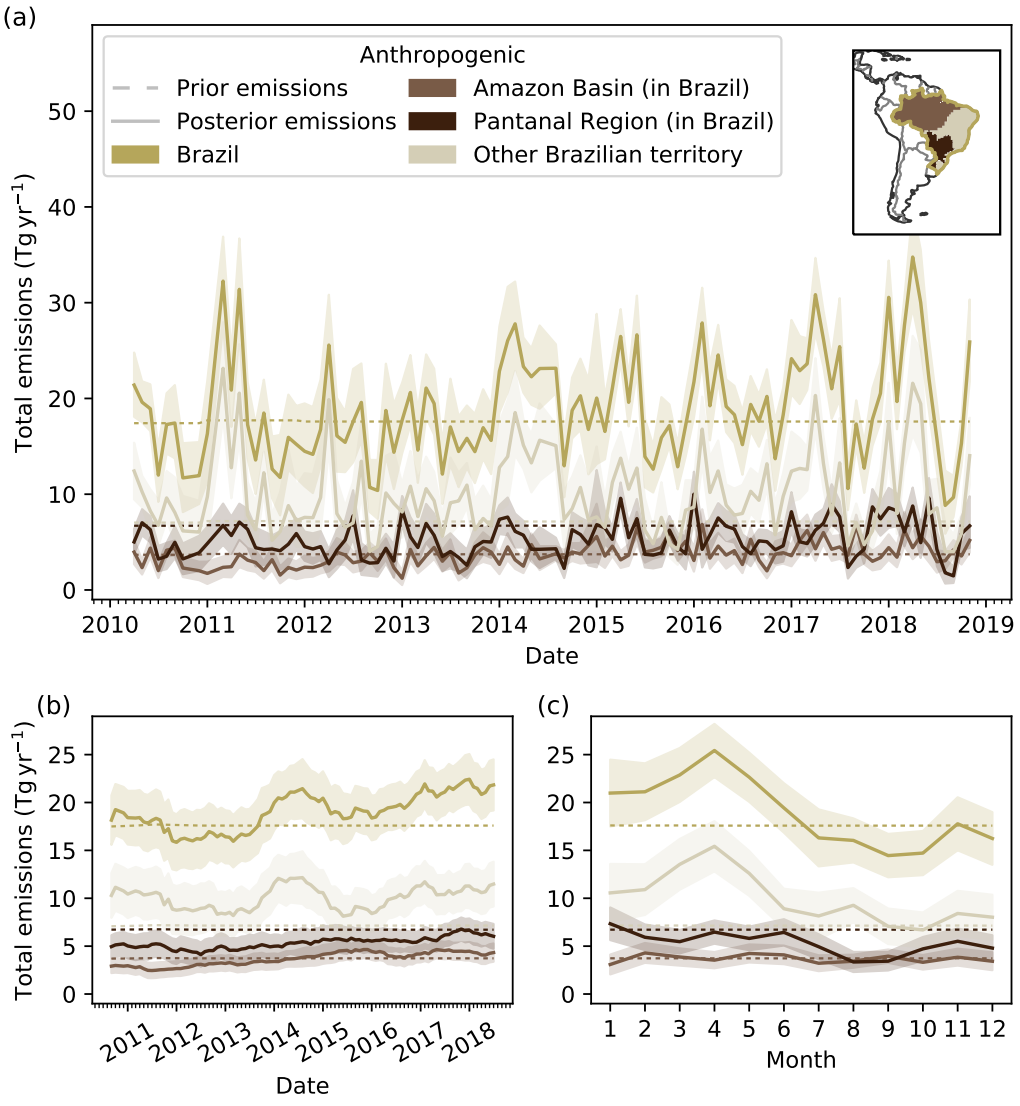

Figure 6. Brazil's anthropogenic emissions aggregated over the Amazon basin, Pantanal region and the rest of Brazilian territory. (a) Monthly emissions with an inset map showing the masks used to delineate different regions, (b) monthly emissions smoothed with a 12-month rolling mean and (c) seasonal means across the 2010 to 2018 period. Errors for mean values assume a 50% correlation between individual months.

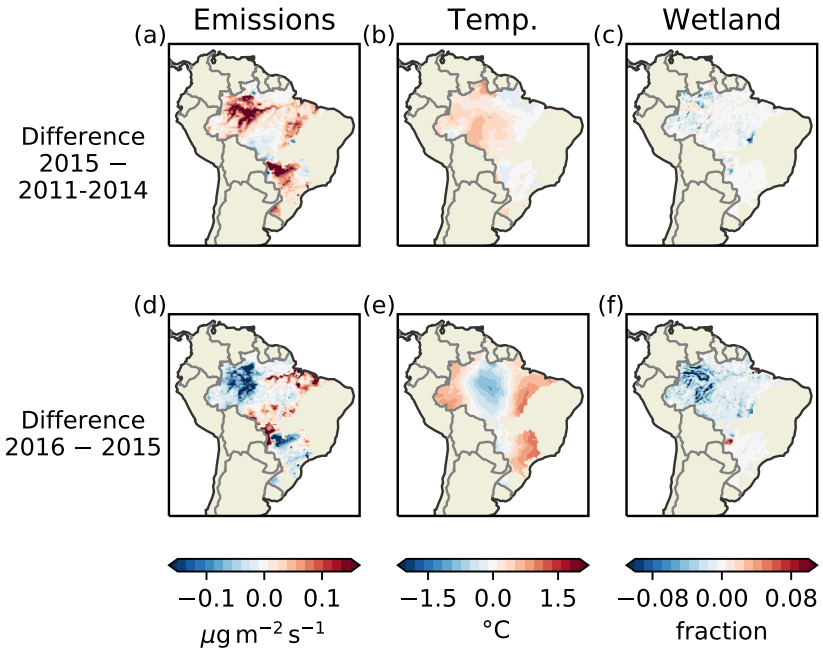

Figure 7. Differences during the wet season (FMA). (a-c) 2015 minus 2011–2014 average, and (d-f) 2016 minus 2015. (a,d) CH_4 emissions, (b,e) surface temperature from the WFDEI meteorological dataset, and (c,f) SWAMPS wetland fraction. All regions outside of the Brazilian Amazon and Pantanal have been masked for clarity.

We find that the increase in 2015 originates mainly from the Western Amazon with a rise of $3.7 \pm 2.7\,\mathrm{Tg\,yr^{-1}}$ (defined as the Brazilian Amazon area west of $-55°$E). This coincides with increased surface temperatures from this region. Wetland extent did not significantly change in the Western Amazon between 2015 and preceding years. Emissions then decrease after mid-2015 to levels that are sustained from 2016–2018. We find that this decrease is correlated with both lower soil temperatures and decreased inundation. The *a priori* emissions may be simulating the decrease after 2016 because the *a priori* emissions are constrained to the observational inundation fields. However, these results suggest that there may be uncertainties in the wetland model temperature sensitivity.

3.3 Validation against ground-based data

We used independent data from ATTO to assess the robustness of our inversion results and to understand what factors are important for the inversion setup. The results of these tests can be seen in Fig. 8. Other datasets besides ATTO exist, such as aircraft data from the Amazon (Wilson et al., 2016; Pangala et al., 2017), but were not available for use.

An inversion using only GOSAT data produced a mean difference between modelled ATTO data and measurements of $42.5\,\mathrm{nmol\,mol^{-1}}$ (Figures 8a and 8e). This difference can largely be attributed to modelled boundary conditions that are

consistently elevated throughout the year above the lowest ATTO data. Introduction of the surface baseline station of RPB (Figures 8b and 8f) improved the boundary condition estimation, with the modelled boundary conditions now consistent with ATTO data in most months and lower than ATTO data in months with significant regional emissions (i.e. times when ATTO may not be representative of boundary conditions). Despite consistency with boundary conditions, this setup produced the highest mean difference with ATTO, $67.4\,\mathrm{nmol\,mol^{-1}}$, due to large regional emissions being estimated. The third case, the setup of our main results, which allowed for an offset between the GOSAT and RPB measurements to be estimated in the inversion, resulted in the best fit to ATTO (Figures 8c and 8g). The model achieved consistent boundary conditions and the smallest mean difference with ATTO ($18.9\,\mathrm{nmol\,mol^{-1}}$). In our inversions from 2010–2018, we estimate a mean offset parameter between GOSAT and RPB data of $22 \pm 8\,\mathrm{nmol\,mol^{-1}}$. The numbers presented for the offsets are a combination of any bias between the data themselves, but also in the model's interpretation of these data sets. The model simulates the three-dimensional atmospheric fields necessary to combine these two datasets together. However, the interpretation of these tests show that near-surface data that help to constrain boundary conditions are required because GOSAT data alone does not have enough resolving power to partition boundary conditions and emissions. An offset parameter should then be included to account for a combination of any differences between in-situ data and satellite data and any offsets due to the atmospheric model.

When our posterior emissions estimates were scaled to match previous results derived by Wilson et al. 2016 (but keeping the posterior boundary conditions fixed from our main results), a larger offset from ATTO of $45.4\,\mathrm{nmol\,mol^{-1}}$ (Figures 8d and 8h) again resulted. This test indicates that larger emissions from the Amazon are inconsistent with ATTO and its representation by the NAME model.

To assess the possibility of large systematic uncertainties in NAME, we show a comparison of the validation at ATTO generated using NAME (as in Figure 8c) with those generated using FLEXPART. This comparison is shown in Appendix Fig. A5 and shows that the posterior emissions and boundary conditions derived here are consistent with ATTO across both models. These results provide additional confidence in the magnitude of emissions that we derive.

3.4 Sensitivity studies

3.4.1 Sensitivity to *a priori* emissions

Sensitivity tests to the effect of different wetland distributions are shown in Fig. 9. Total emissions do not change significantly between these sensitivity tests, despite the large seasonal cycle in the *a priori* WetCHARTS emissions that is not reflected in the other wetland distributions. This suggests that the inversion is well-constrained by the atmospheric data and is not significantly influenced by the prior. There are small differences in wetland and anthropogenic partitioning, but emissions are consistent within uncertainties.

In addition to different *a priori* wetland distributions, sensitivity tests to perturb *a priori* emissions from each source sector are shown in Appendix Figures A6, A7 and A8. The main impact of perturbing *a priori* emissions from any source sector comes in the partitioning of total emissions into the sources, particularly between anthropogenic and wetland emissions. This is due to a small overlap between anthropogenic and wetland sources (Figures 2 and 3). However, the trade-off between these

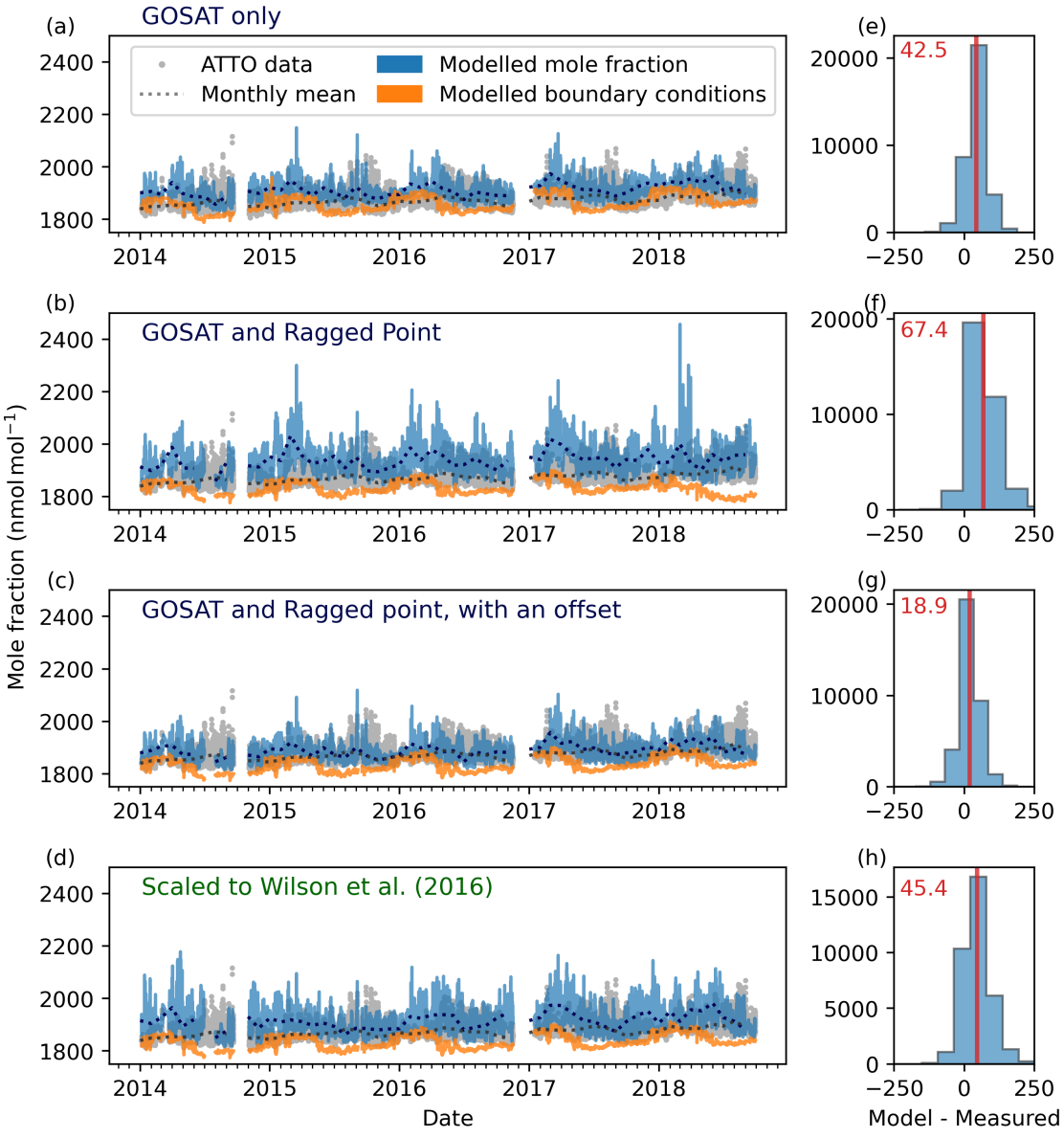

Figure 8. (a-d) Comparison of modelled and measured mole fractions at ATTO for different posterior emissions with (e-h) histograms of the differences. Posterior emissions derived in inversions using (a,e) GOSAT measurements only, (b,f) both GOSAT and RPB data but no offset parameter in the inversion, and (c,g) both GOSAT and RPB data and with an offset parameter between the two data sets in the inversion . (d,h) Posterior emission distribution of our main results but scaled so that total CH_4 emissions in the Brazilian Amazon was equivalent to those derived in Wilson et al. (2016).

two sectors is smaller than the initial perturbation to the prior and emissions are still consistent within confidence intervals, suggesting that the sectoral partitioning is robust. The largest sensitivity to the *a priori* emissions is shown when doubling *a priori* biomass burning emissions (Fig. A8) and the resulting posterior biomass burning estimate is not consistent within uncertainties to the unperturbed case. Overall, these tests show that our results and the associated sectoral partitioning, with the exception of some influence from the biomass burning prior, are robust to the *a priori* emissions used.

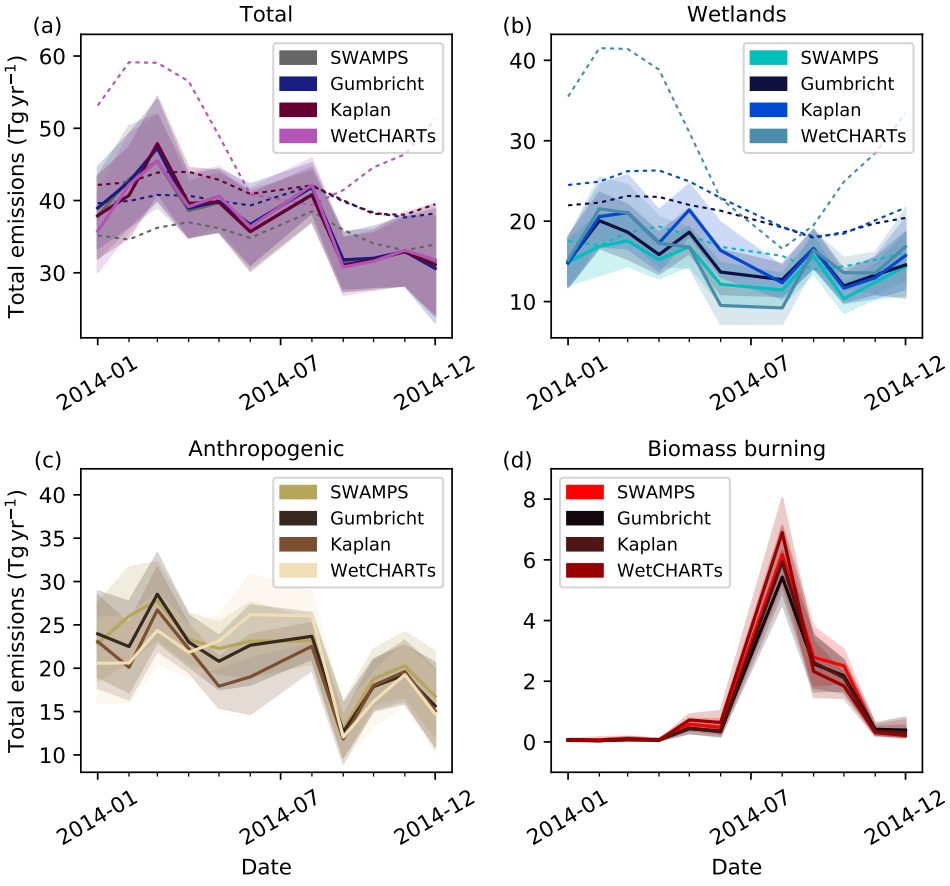

Figure 9. Brazil's CH_4 emissions in a sensitivity inversion using perturbed *a priori* wetland distributions. All other components were held at the original configuration. Total emissions for all of South America were scaled to $44\,\mathrm{Tg\,yr^{-1}}$ for all distributions apart from WetCHARTs, which used its derived emissions. (a) Total, (b) wetland, (c), anthropogenic, and (d) biomass burning emissions. Prior emissions are only shown in (a, b) as they only vary for these components in this test.

3.4.2 Influence of *a priori* boundary conditions

Results of using a different global model of *a priori* boundary conditions are shown in Appendix Fig. A9. Due to differences in the seasonal cycle when comparing the CAMS and MOZART boundary conditions in 2014, this analysis was run for the full 2010–2018 period to provide a longer comparison. While there is some month to month variability, the overall patterns are consistent between the two inversion setups, suggesting that the inversion is robust to the *a priori* boundary conditions. As demonstrated in Section 3.3, it is important to include data that can help the inversion constrain the boundary conditions, through, for example, surface measurements from remote background stations.

3.4.3 Influence of model XCO_2 on XCH_4

We generated ten variations of the XCH_4 dataset used in the inversion based on different model XCO_2. Figure 10 shows the emissions estimates that result when perturbing XCH_4 by random values of the model XCO_2 used to generate XCH_4 using the CO_2 proxy method. Because of some differences in 2014, this analysis was run for the full 2010–2018 period.

Across the ten variations, mean emissions over 2010–2018 range from 33.8–34.8 $\mathrm{Tg\,yr^{-1}}$ in total, 19.0–19.4 $\mathrm{Tg\,yr^{-1}}$ for anthropogenic, 13.0–13.4 $\mathrm{Tg\,yr^{-1}}$ for wetlands and 1.7–1.8 $\mathrm{Tg\,yr^{-1}}$ for biomass burning. Individual months can exhibit larger ranges in the ten variants, in some cases spanning $> 10\,\mathrm{Tg\,yr^{-1}}$. The differences based on model XCO_2 does not exhibit any particular seasonality. The change between the 2011–2013 and 2014–2018 periods across these ten inversions produces a range of 5.9–7.0 $\mathrm{Tg\,yr^{-1}}$. Thus, the increase in emissions is robust to uncertainties in XCO_2.

4 Discussion

We find that Brazil's emissions increased during 2014–2018 over 2011–2013 levels by $6.9 \pm 5.3\,\mathrm{Tg\,yr^{-1}}$ and this coincides with a large increase in global CH_4 mole fraction growth rate in 2014 (Nisbet et al., 2019). The increase in Brazil's emissions is primarily driven by anthropogenic and wetland sources. Brazil's anthropogenic emissions are dominated by agriculture and mainly cattle, which is likely to be the main source for the inferred anthropogenic change. However, we did not have sufficient information with which to robustly separate total anthropogenic emissions into individual sub-sectors. Future work should couple measurements of δ^{13}C-CH_4 from Brazil along with campaigns to sample representative isotopic source signatures (Ganesan et al., 2018) to better understand whether changes in these sources are consistent with isotopic constraints.

The increased wetland emissions that we derive in the wet season of 2015 primarily originates from the Western Amazon. Previous studies have found that changes in wetland CH_4 emissions exhibit complex dynamics during El Niño years. Zhang et al. (2018) found through model simulations that the 2015–2016 El Niño led to larger instantaneous growth in CH_4 emissions than previous El Niño periods. This study also showed that there was a large increase in the Western Amazon due to increased soil respiration from high soil temperatures, despite a decline in wetland extent due to drought. This pattern is consistent with the results that we have derived from atmospheric data rather than from model simulations. In contrast to Zhang et al. (2018), which also found a 2015–2016 El Niño effect on Western Amazon emissions, we find that emissions increased during the 2015

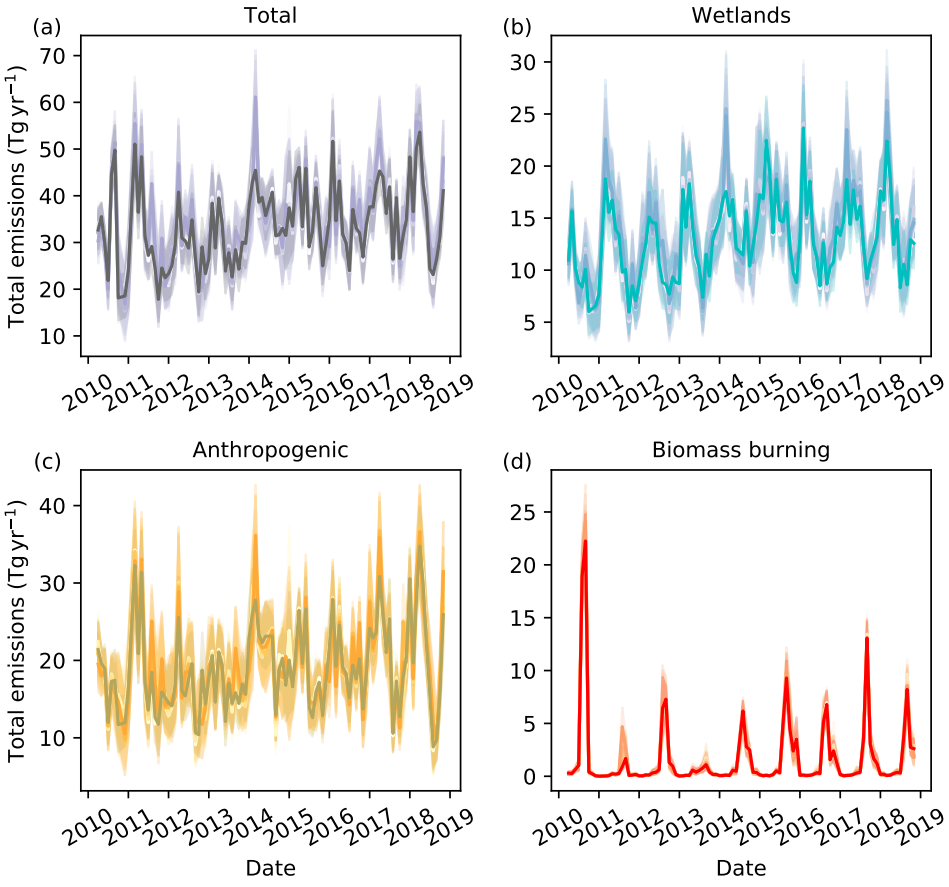

Figure 10. Brazil's CH_4 emissions in a sensitivity inversion using ten variants of GOSAT data generated with different model XCO_2. All other components were held at the original configuration. Each line represents a different inversion run. (a) Total, (b) wetland, (c), anthropogenic, and (d) biomass burning emissions. Prior emissions do not vary in this test.

wet season rather than the 2016 wet season. We instead show a decline in 2016 emissions, surface temperature and wetland extent compared to 2015 levels. This discrepancy in temporal response from Zhang et al. (2018), suggests that the dynamics of the wetland response to climatic perturbations may require further investigation.

Our results show that emissions can be derived for a country of the size of Brazil from satellite data coupled with high-
350 resolution atmospheric transport modelling, but careful consideration needs to be paid to the setup of the inversion. Regional inversions use atmospheric data to estimate boundary conditions and regional emissions. Due to the lower signal-to-noise of GOSAT data (which are sensitive to surface emissions that are mixed through the entire atmospheric column) compared to ground-based data (although the reduced surface sensitivity and precision of satellite data needs to be weighed against the greater geographical coverage), we find that additional surface data is required to better constrain the boundary conditions.

However, we find that when combining satellite data with calibrated surface data in an inversion it is critical to incorporate an offset parameter between the two datasets in the inversion. The GOSAT product used here has been previously corrected by $7.7\,\mathrm{nmol\,mol^{-1}}$ as a global average offset to independent ground based measurements from the Total Carbon Column Observing Network (TCCON) (Wunch et al., 2011). However, large regional variations can still exist (Dils et al., 2014). The estimated offset in an inversion is due to biases between the different datasets as well as their representation by the atmopsheric transport model. Other inversion studies have imposed latitude-dependent bias corrections on other GOSAT data (Bergamaschi et al., 2009; Turner et al., 2015).

Janardanan et al. (2020) estimated Brazil's CH_4 emissions using a coupled global Eulerian–Lagrangian model from 2011–2017 using GOSAT and surface data and find total emissions to be $56.2\,\mathrm{Tg\,yr^{-1}}$ compared with $33.3 \pm 3.7\,\mathrm{Tg\,yr^{-1}}$ derived in this study. The difference between our results can be attributed to the natural wetland emissions estimates for which Janardanan et al. (2020) derive $39.8 \pm 12.4\,\mathrm{Tg\,yr^{-1}}$ compared to $13.1 \pm 1.9\,\mathrm{Tg\,yr^{-1}}$ presented here. Anthropogenic estimates (excluding biomass burning) are similar at $16.5\,\mathrm{Tg\,yr^{-1}}$ compared with our estimate of $18.8 \pm 2.6\mathrm{Tg\,yr^{-1}}$. One factor in this difference could be the differing GOSAT retrieval products used which were derived using different algorithms (CO_2 proxy vs full physics retrievals). Another reason for the discrepancy could stem from Janardanan et al. (2020) not allowing for an offset parameter between the surface/aircraft and satellite data within their inversion. In the case where we similarly set up our inversion to not include an offset parameter (as shown by the ATTO comparison in Fig. 8b), we also derive larger total emissions of $51.7 \pm 3.5\mathrm{Tg\,yr^{-1}}$ for 2014. Not allowing for this offset produces the poorest comparison to the independent ATTO measurements. However, it is important to note that our validation is based on only one site because of the availability of data.

Studies deriving Amazon Basin CH_4 emissions using aircraft data from within the Amazon are also higher than than our estimates at $49\,\mathrm{Tg}\ (\mathrm{yr^{-1}}$, Miller et al. 2007; Wilson et al. 2016). However, these higher estimates, as shown in Fig. 8d, when simulated with NAME, are less consistent when compared with CH_4 mole fractions measured at the ATTO tower. The wetland results presented here are most consistent with the lower bound estimates from Saunois et al. (2016) which range from 23.4–63.7 within Tropical South America. As discussed in Section 3.4.1, neither varying the magnitude of the prior input for wetlands nor the wetland extent map used, significantly altered our posterior estimates.

We propose one reason for the difference from aircraft based estimates could be that the studies using aircraft data may not be able to constrain emissions over the whole of the Amazon Basin and furthermore, at the country-scale, though our comparison at present has only been validated by one in situ measurement station. Future work should perform a detailed comparison between aircraft-derived estimates and those derived from satellites, investigating the inversion setup and the degree of constraint by the datasets to understand the reasons for this discrepancy. The main benefit of using satellite data is in its widespread coverage, which allows for country-scale emissions to be derived (albeit, with inclusion of calibrated near-surface data in the inversion).

Overall, we derive lower emissions than previous studies. We show the validation of our results at ATTO using two models, NAME and FLEXPART. The consistency between the two models in simulating the magnitude of mole fractions at ATTO provides some confidence in the lower emissions we derive over previous studies. In future, performing a full set of inversion results using a large range of models with different physical parameterisations could help to quantify the magnitude of any systematic uncertainties.

5 Conclusions

We estimated Brazil's CH_4 emissions from 2010–2018 using a combination of GOSAT satellite data and surface data from Ragged Point, Barbados. Due to the spatial and temporal separation in the three main sources of Brazil's emissions (anthropogenic, wetland and biomass burning), we were able to derive emission estimates by sector.

We find mean emissions from 2010–2018 to be $33.6 \pm 3.6\,\mathrm{Tg\,yr^{-1}}$, corresponding to $19.0 \pm 2.6\,\mathrm{Tg\,yr^{-1}}$ from anthropogenic, $13.0 \pm 1.9\,\mathrm{Tg\,yr^{-1}}$ from wetland and $1.7 \pm 0.3\,\mathrm{Tg\,yr^{-1}}$ from biomass burning. We find a rise of $6.9 \pm 5.3\,\mathrm{Tg\,yr^{-1}}$ occurring between 2011–2013 and 2014–2018 periods. Both anthropogenic and wetland sources drive the increase in emissions over the period. This rise in emissions occurred during a period of accelerated global CH_4 growth, suggesting that Brazil's CH_4 sources have a significant influence on changes in the atmosphere.

We find that wetland emissions from the Western Amazon increased by $3.7 \pm 2.7\,\mathrm{Tg\,yr^{-1}}$ in the 2015 wet season, at the start of the 2015–2016 El Niño, and decreased subsequently from 2016. We show that the increase is likely to be driven by increased surface temperatures and thus, respiration rates, rather than through changes in inundation.

Our study demonstrates that satellite data, with its enhanced coverage compared to surface data, can be used to infer country-scale emissions. This is beneficial for independently comparing top-down estimates with national reports to the UNFCCC. However, we show that satellite data must be used in conjunction with calibrated surface data, which provide critical constraints on boundary conditions in regional inversions. It is also necessary to account for any offsets between datasets which can result from either biases between satellite data and surface data or from the atmospheric transport model used to simulate these data. Otherwise the resulting emission estimates may be biased. Our sensitivity studies show that our emissions estimates are insensitive to most inputs, but the largest differences are driven by uncertainties in the model XCO_2 used to derive XCH_4.

Code and data availability. University of Leicester GOSAT Proxy XCH_4 data can be accessed via the Copernicus Climate Data Store or by contacting Rob Parker. RPB data can be accessed from https://data.ess-dive.lbl.gov/view/doi:10.3334/CDIAC/ATG.DB1001 and by contacting Dickon Young. ATTO data can be accessed from https://www.attodata.org/ and by contacting Jošt Lavrič. The inversion code and NAME footprints used in this study can be accessed by contacting Rachel Tunnicliffe and Anita Ganesan.

Appendix A

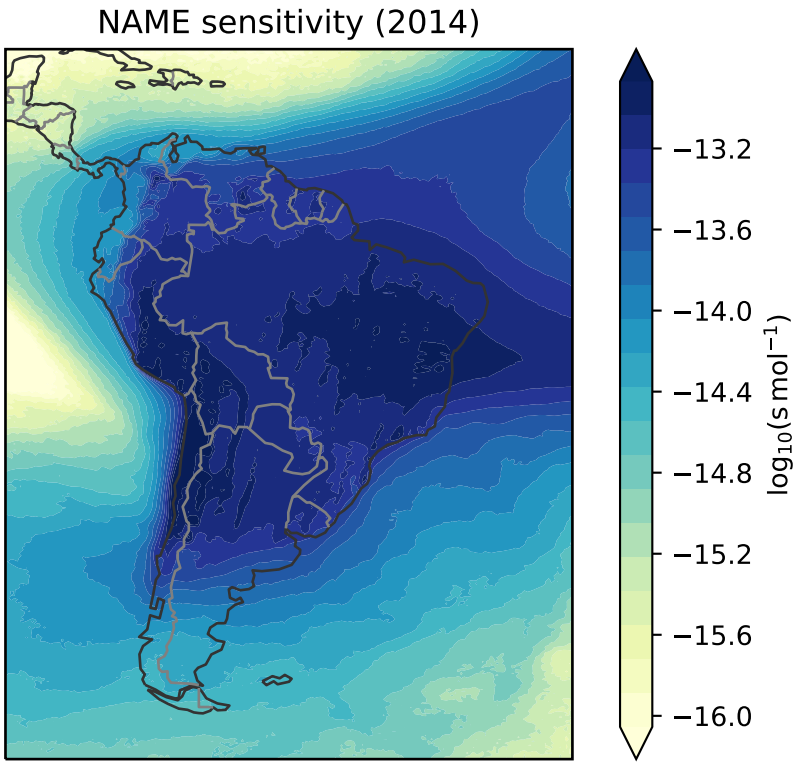

Figure A1. Annual mean NAME sensitivity map for GOSAT measurements in nadir mode within the area -35.8 to 7.3°N and -76.0 to -32.8°E over Brazil, for 2014.

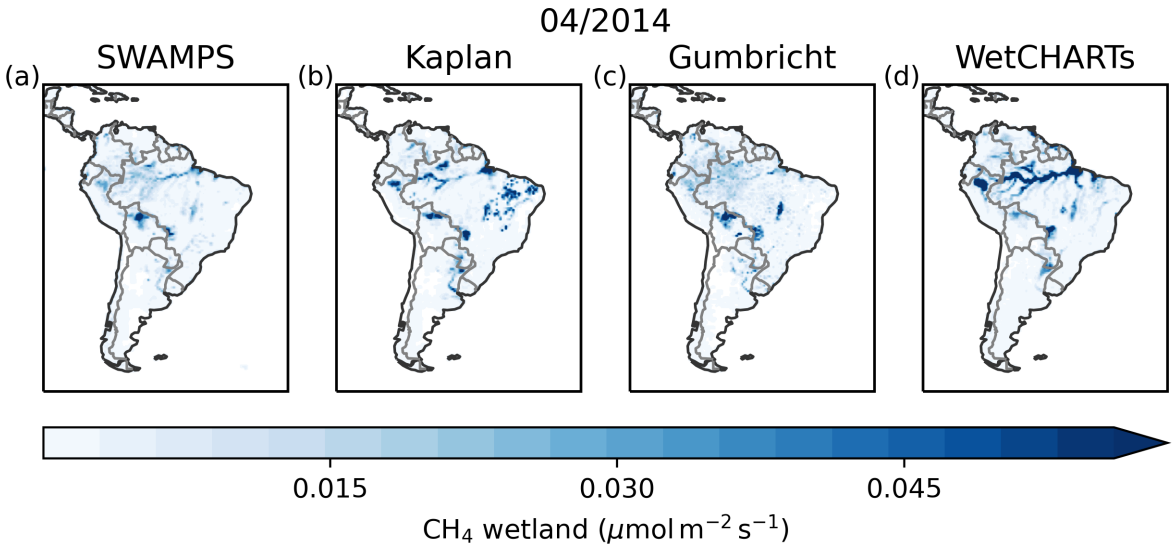

Figure A2. CH_4 emissions for each of the four *a priori* wetland emissions used in the wetland extent sensitivity study. Panels (a)-(c) SWAMPS, Kaplan and Gumbricht fractional maps are combined with the JULES emissions output. Details of these inversion setups are described in Table 2. This is shown for April, 2014 which is a wet season month with high emissions in the Amazon basin and the Pantanal region.

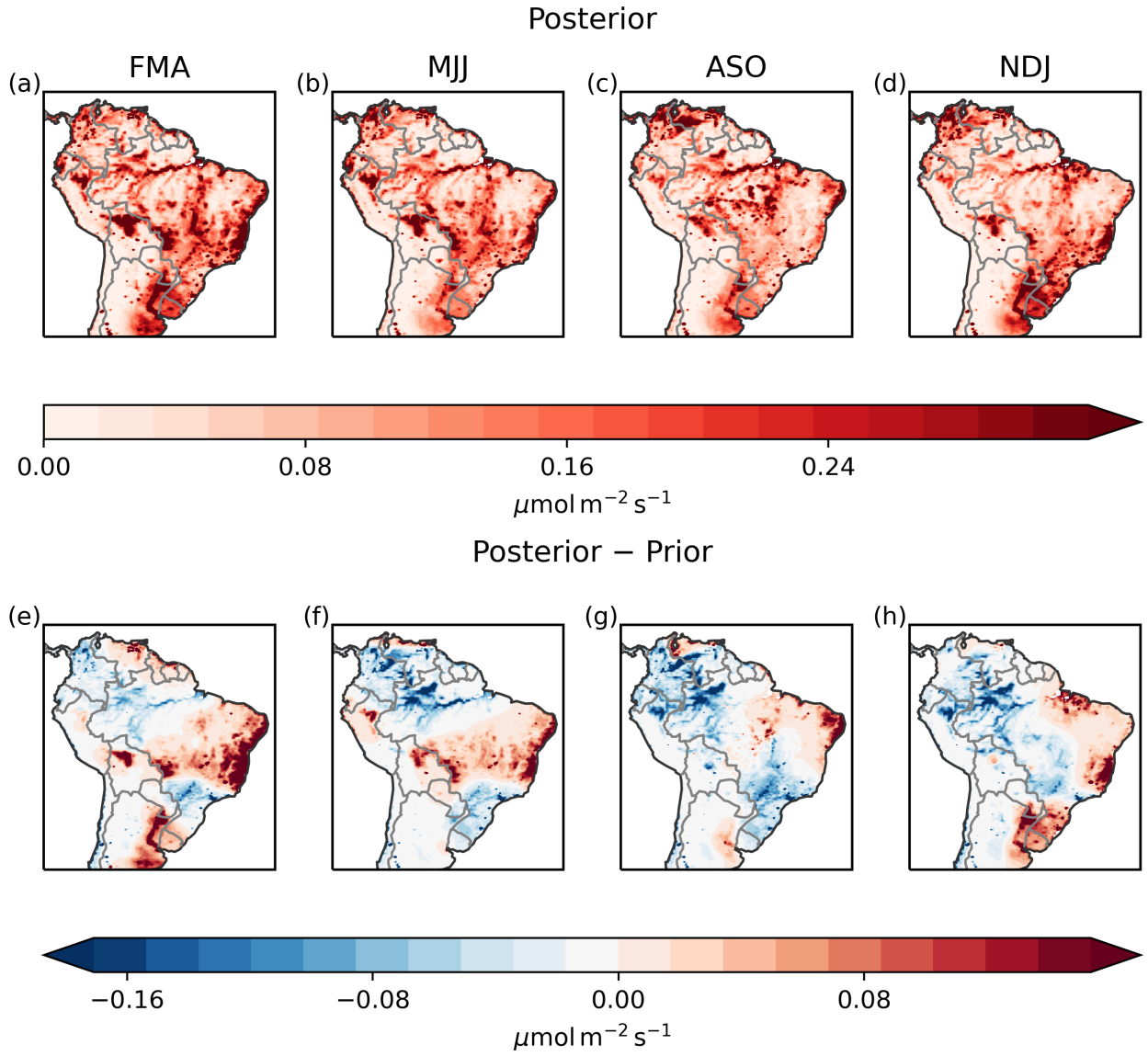

Figure A3. Emissions maps across 2011–2018 time period grouped into February-April (FMA), May-July (MJJ), August-October (ASO) and November-January (NDJ). Panels (a)-(d) CH_4 posterior emissions maps and (e)-(h) difference between the posterior and the *a priori* emissions input.

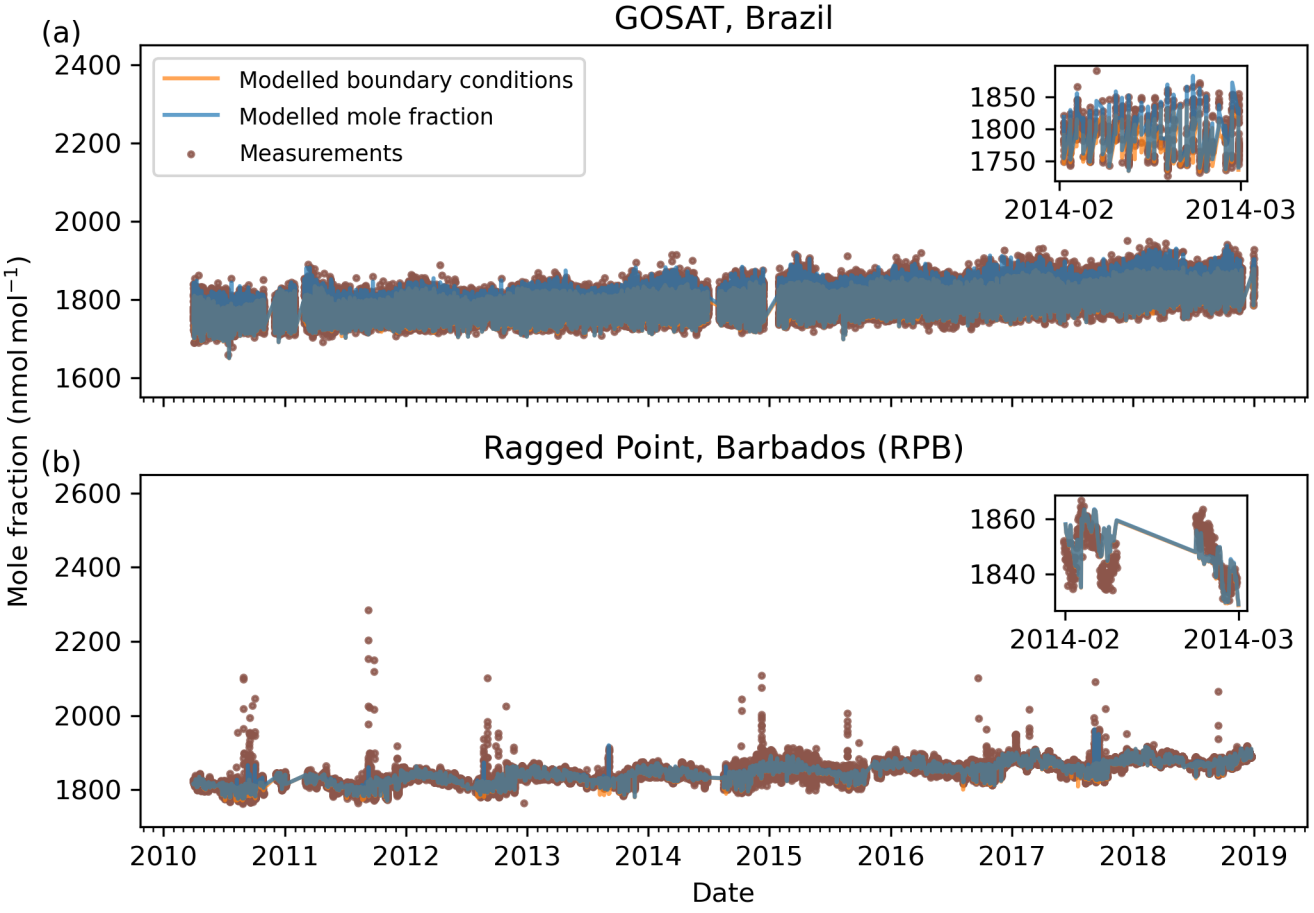

Figure A4. Modelled mole fractions derived from the posterior emissions estimate compared to measurements from (a) GOSAT and (b) RPB. The orange line shows posterior boundary conditions and the blue line shows the total modelled mole fraction. Measurements are displayed as red dots.

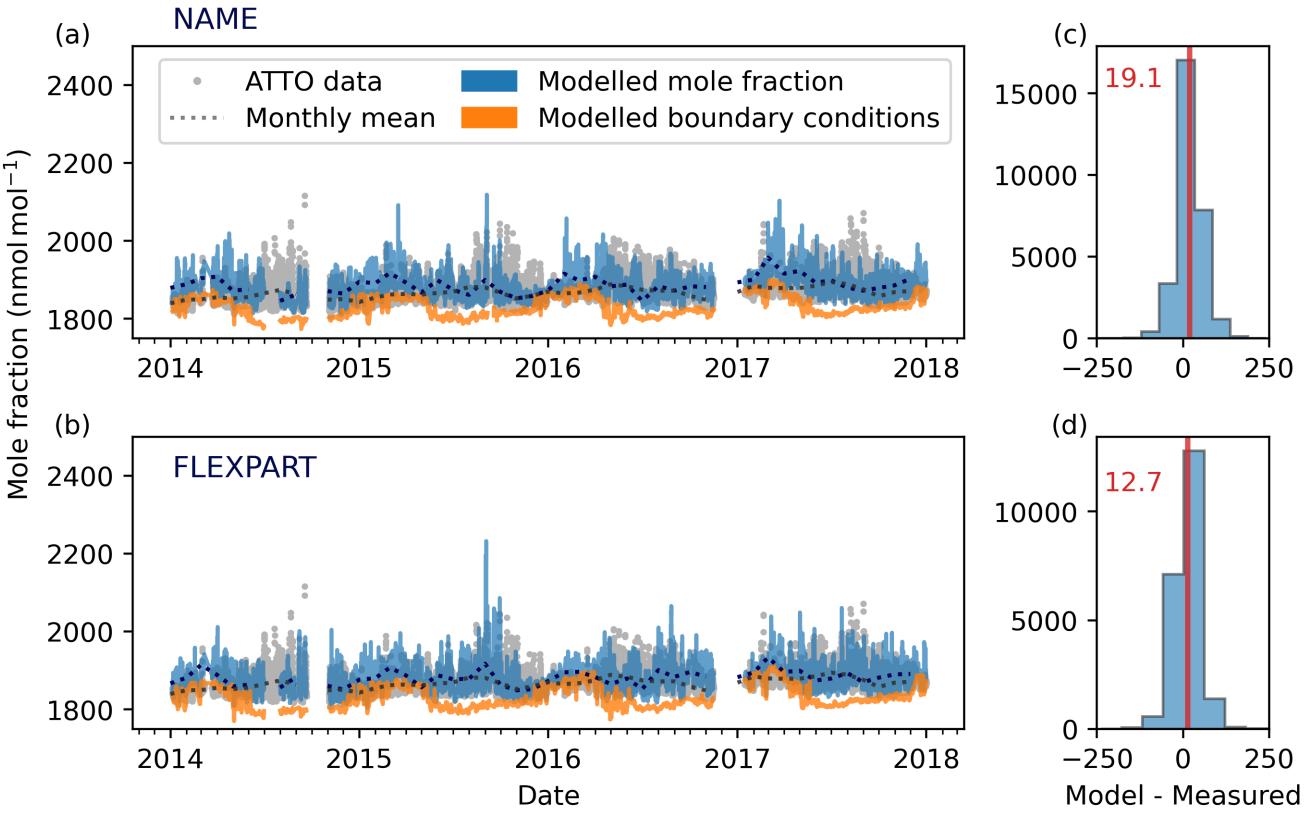

Figure A5. Comparison of modelled and measured mole fractions at ATTO with the same posterior emissions and boundary conditions convolved with sensitivity maps derived from two different models. (a) NAME model (main results) and (b) FLEXPART model where (c-d) shows histograms of the difference. Posterior emissions were derived from our inversion setup using both GOSAT and RPB data with an offset parameter between the two data sets allowed within the inversion.

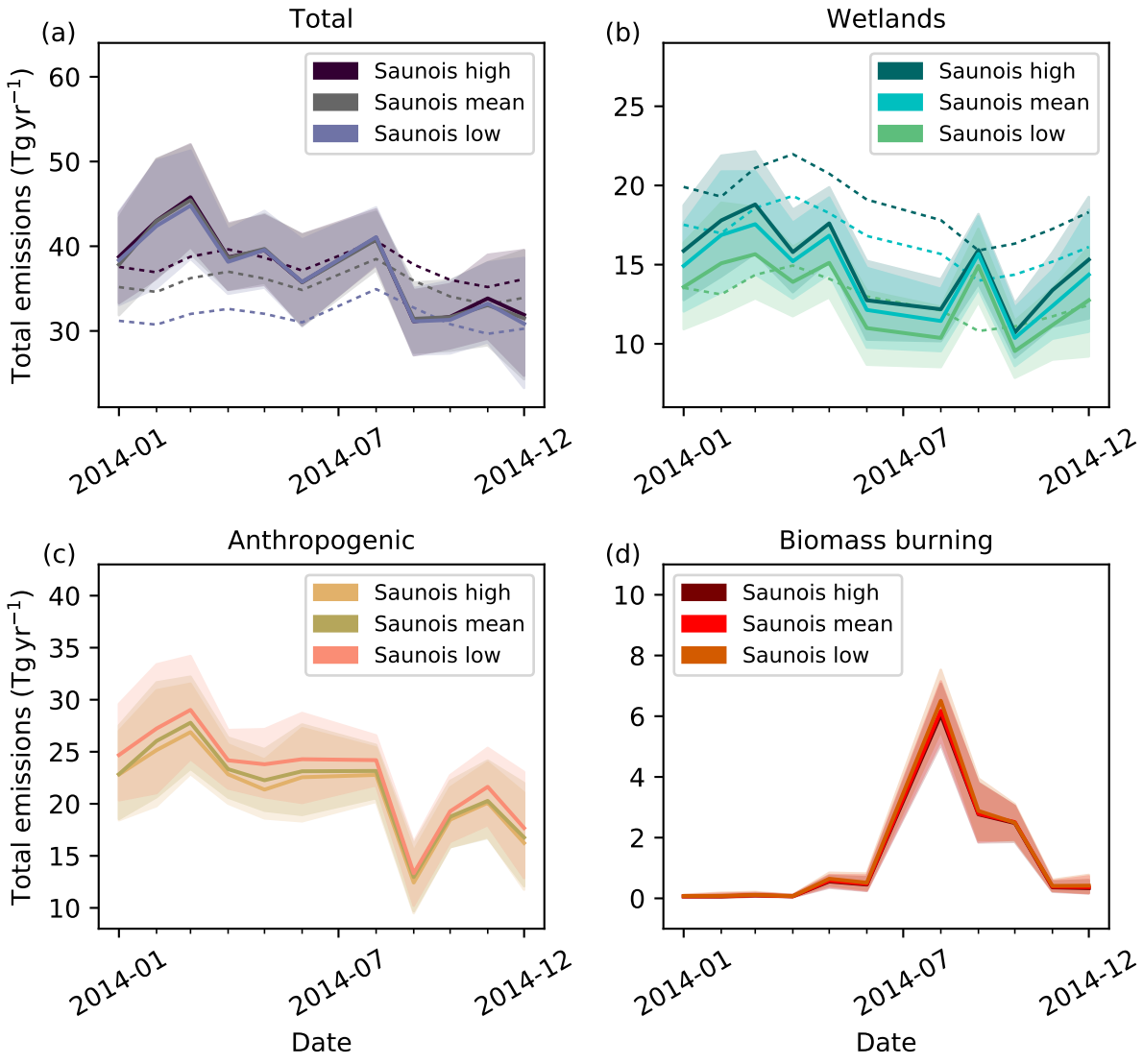

Figure A6. Brazil's CH_4 emissions in a sensitivity inversion using a perturbed *a priori* wetlands emissions magnitude. All other components were held at the original configuration. *A priori* wetland emissions for all of South America were scaled to 32 (low), 44 (mean) or 50 (high) $\mathrm{Tg\,yr^{-1}}$ (as defined for Tropical South America in Saunois et al. 2016). (a) Total, (b) wetland, (c), anthropogenic, and (d) biomass burning emissions. Prior emissions are only shown in (a, b) as they only vary for these components in this test.

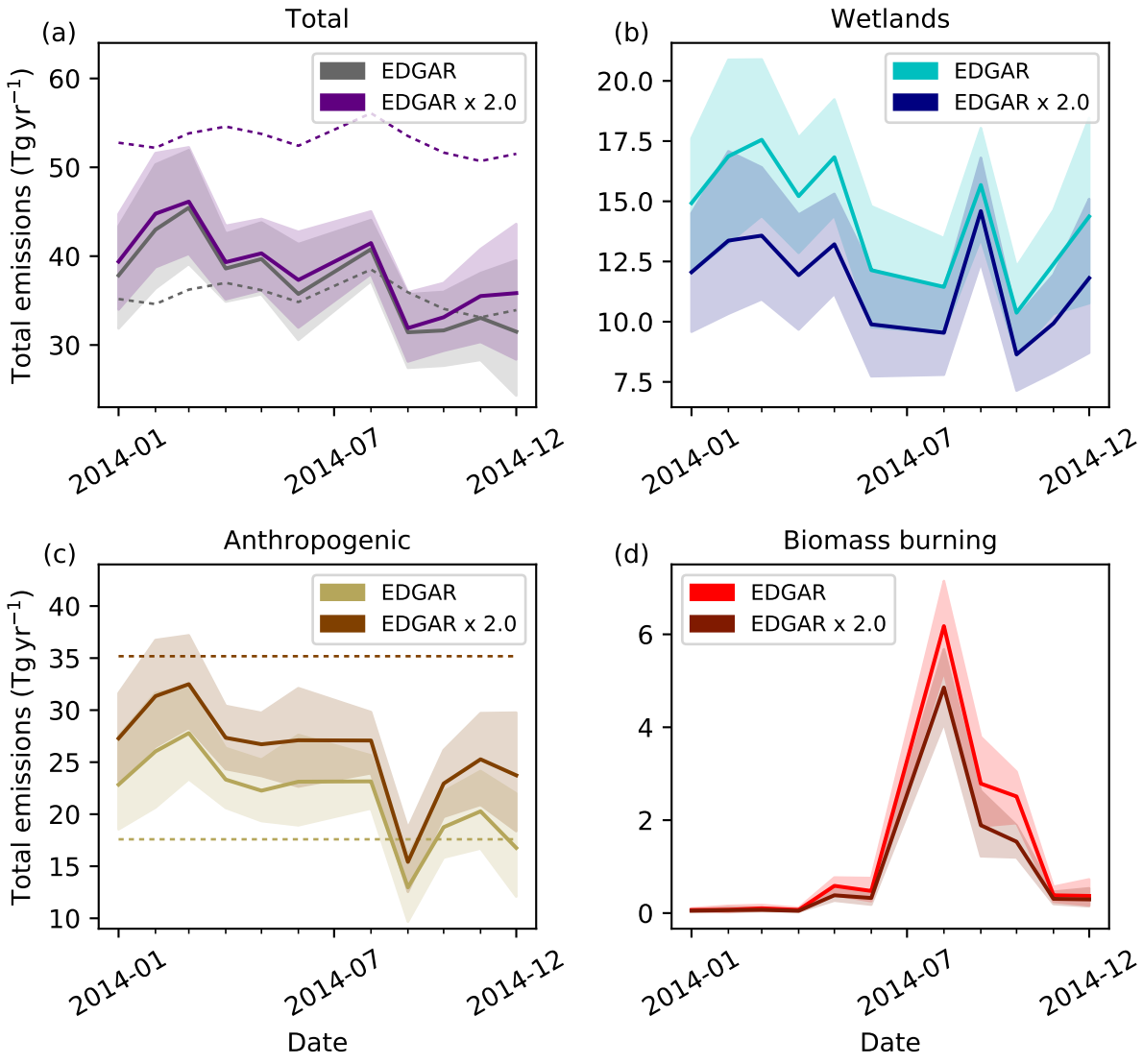

Figure A7. Brazil's CH_4 emissions in a sensitivity inversion using perturbed *a priori* anthropogenic emissions. All other components were held at the original configuration. Anthropogenic emissions for all of South America were doubled from EDGAR. (a) Total, (b) wetland, (c), anthropogenic, and (d) biomass burning emissions. Prior emissions are only shown in (a, c) as they only vary for these components in this test.

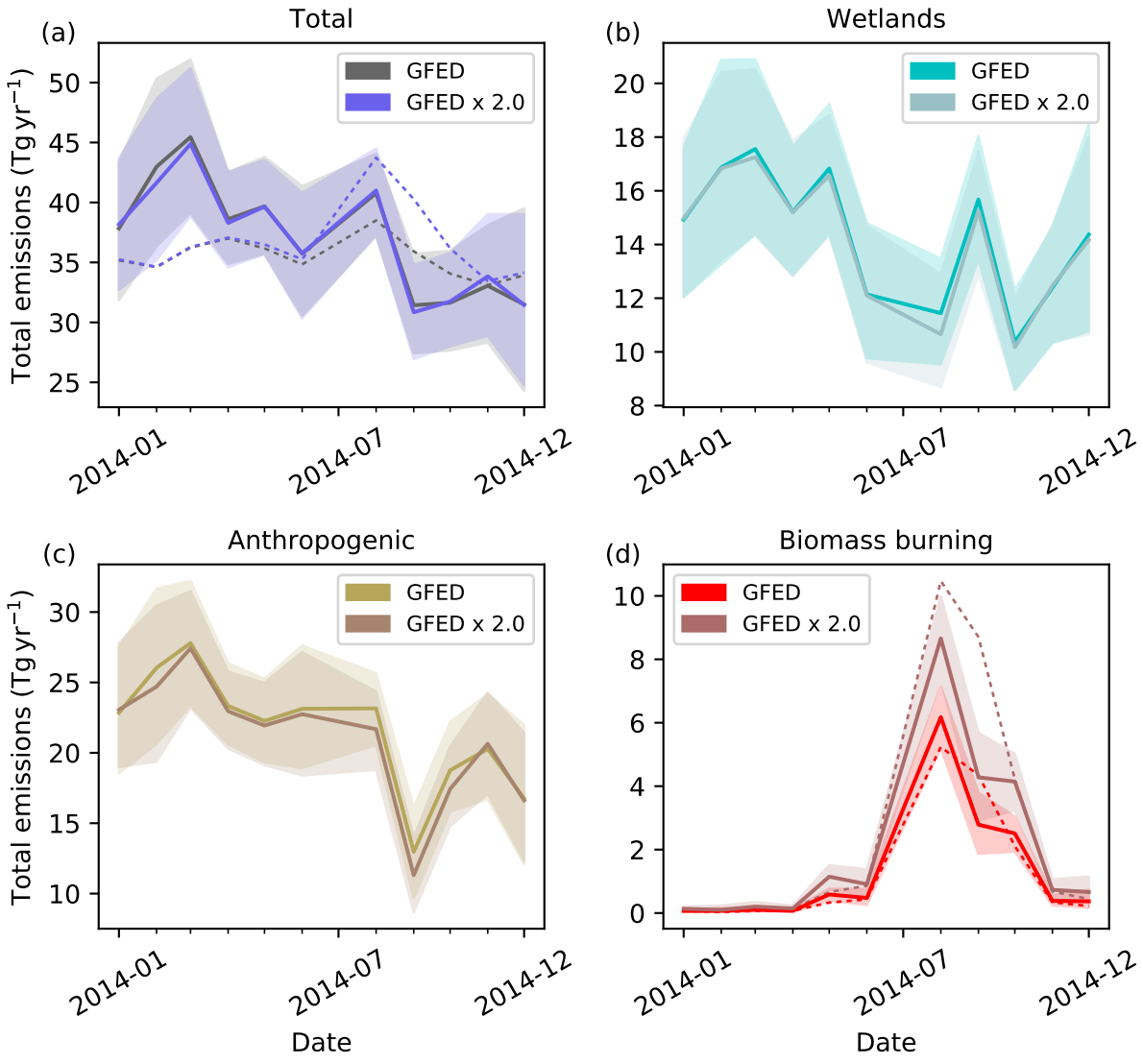

Figure A8. Brazil's CH_4 emissions in a sensitivity inversion using perturbed *a priori* biomass burning emissions. All other components were held at the original configuration. Biomass burning emissions for all of South America were doubled from GFED. (a) Total, (b) wetland, (c), anthropogenic, and (d) biomass burning emissions. Prior emissions are only shown in (a, d) as they only vary for these components in this test.

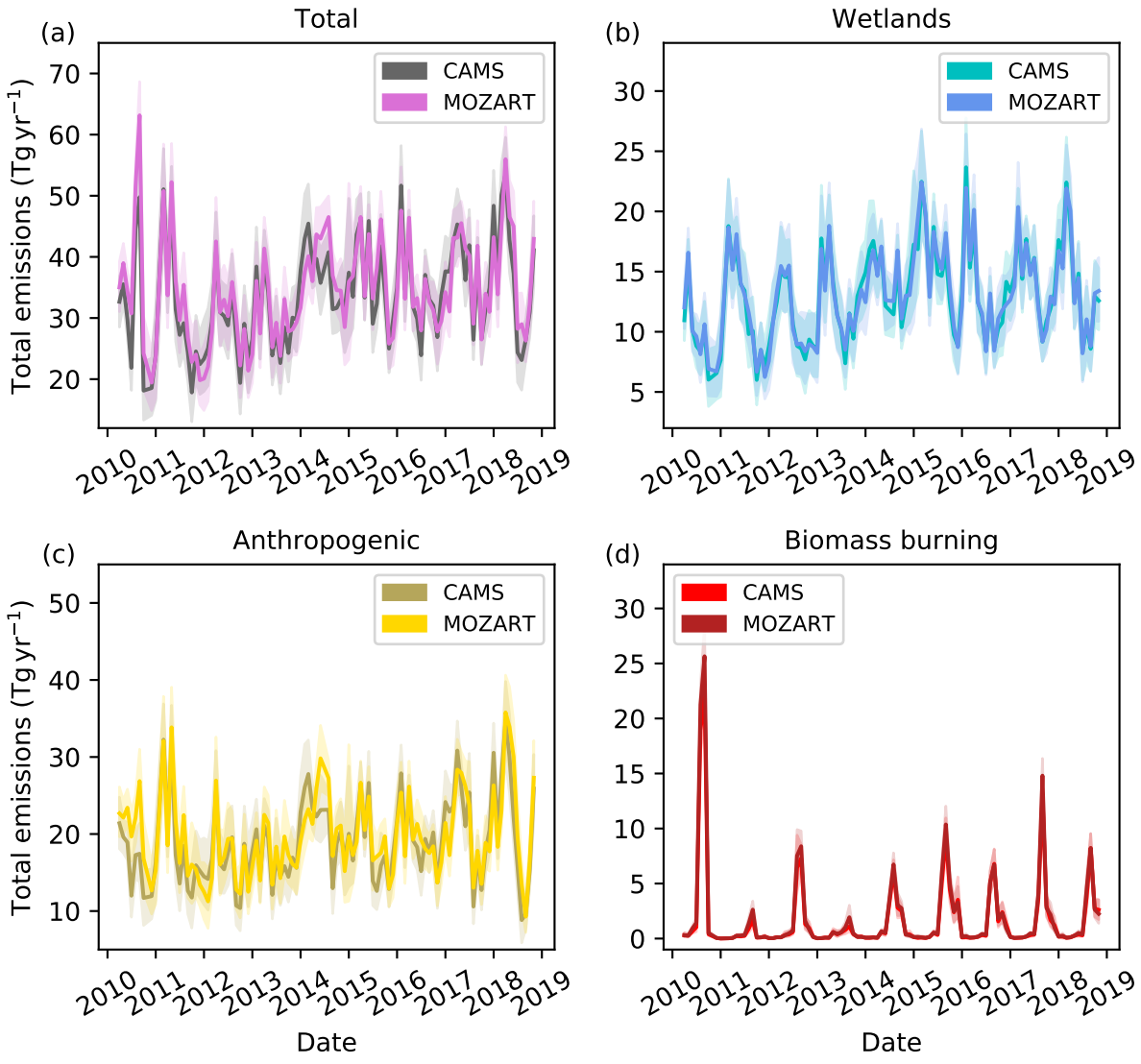

Figure A9. Brazil's CH_4 emissions in a sensitivity inversion using perturbed *a priori* boundary conditions from the MOZART model. All other components were held at the original configuration. (a) Total, (b) wetland, (c), anthropogenic, and (d) biomass burning emissions. *A priori* emissions do not vary in this test.

Author contributions. R.T and A.G designed the methodology and wrote the manuscript. R.T performed the analysis. R.P and H.B provided the GOSAT data. N.G provided JULES CH_4 emission fields. B.P. and Z.Z. provided SWAMPS wetland extent maps. J.L and D.W. provided data from the Amazon Tall Tower Observatory. M.R advised on methodology. D.Y and S.O. provided data from Ragged Point, Barbados.

Competing interests. We declare no conflicts of interest.

Acknowledgements. This work and its contributors (R.T) were supported by the Newton Fund through the Met Office Climate Science for Service Partnership Brazil (CSSP Brazil) and the Natural Environment Research Council (NERC) Methane Observations and Yearly Assessments programme (MOYA, NE/N016548/1). A.G was funded by the NERC Independent Research Fellowship NE/L010992/1. R.J.P and H.B were funded via the UK National Centre for Earth Observation (NCEO grant number: nceo020005).

We thank the Japanese Aerospace Exploration Agency, National Institute for Environmental Studies, and the Ministry of Environment for the GOSAT L1B data and their continuous support as part of the Joint Research Agreement. We thank Alistair Manning (Met Office) for useful and insightful discussions about this work.

The operation of the Ragged Point site was funded by the National Aeronautical and Space Administration (NASA, USA) (grants NAG5-12669, NNX07AE89G and NNX11AF17G to MIT; grants NAG5-4023, NNX07AE87G, NNX07AF09G, NNX11AF15G and NNX11AF16G to SIO) under the AGAGE programme and the National Oceanic and Atmospheric Administration (NOAA, USA) (contract RA-133R-15-CN-0008 to the University of Bristol). ATTO data were supported by the Max Planck Society (MPG), the German Federal Ministry of Education and Research (contracts 01LB1001A and 01LK1602A) and the Brazilian Ministério da Ciência, Tecnologia e Inovação (MCTI/FINEP contract 01.11.01248.00) as well as the Amazon State University (UEA), FAPEAM, LBA/INPA and SDS/CEUC/RDS-Uatumã. We acknowledge the Swiss Federal Office for Meteorology and Climatology (MeteoSwiss) for providing access to ECMWF ERA-Interim reanalysis products for use with the FLEXPART model. This work was carried out using the computational facilities of the Advanced Computing Research Centre, University of Bristol - http://www.bristol.ac.uk/acrc/. GOSAT retrievals used the ALICE High Performance Computing Facility at the University of Leicester.

References

Andreae, M. O., Acevedo, O. C., Araùjo, A., Artaxo, P., Barbosa, C. G., Barbosa, H. M., Brito, J., Carbone, S., Chi, X., Cintra, B. B., Da Silva, N. F., Dias, N. L., Dias-Júnior, C. Q., Ditas, F., Ditz, R., Godoi, A. F., Godoi, R. H., Heimann, M., Hoffmann, T., Kesselmeier, J., Könemann, T., Krüger, M. L., Lavric, J. V., Manzi, A. O., Lopes, A. P., Martins, D. L., Mikhailov, E. F., Moran-Zuloaga, D., Nelson, B. W., Nölscher, A. C., Santos Nogueira, D., Piedade, M. T., Pöhlker, C., Pöschl, U., Quesada, C. A., Rizzo, L. V., Ro, C. U., Ruckteschler, N., Sá, L. D., De Oliveira Sá, M., Sales, C. B., Dos Santos, R. M., Saturno, J., Schöngart, J., Sörgel, M., De Souza, C. M., De Souza, R. A., Su, H., Targhetta, N., Tóta, J., Trebs, I., Trumbore, S., Van Eijck, A., Walter, D., Wang, Z., Weber, B., Williams, J., Winderlich, J., Wittmann, F., Wolff, S., and Yáñez-Serrano, A. M.: The Amazon Tall Tower Observatory (ATTO): Overview of pilot measurements on ecosystem ecology, meteorology, trace gases, and aerosols, Atmospheric Chemistry and Physics, 15, 10 723–10 776, https://doi.org/10.5194/acp-15-10723-2015, www.atmos-chem-phys.net/15/10723/2015/, 2015.

Beck, V., Gerbig, C., Koch, T., Bela, M. M., Longo, K. M., Freitas, S. R., Kaplan, J. O., Prigent, C., Bergamaschi, P., and Heimann, M.: WRF-Chem simulations in the Amazon region during wet and dry season transitions: Evaluation of methane models and wetland inundation maps, Atmospheric Chemistry and Physics, 13, 7961–7982, https://doi.org/10.5194/acp-13-7961-2013, www.atmos-chem-phys.net/13/7961/2013/, 2013.

Bergamaschi, P., Frankenberg, C., Meirink, J. F., Krol, M., Dentener, F., Wagner, T., Platt, U., Kaplan, J. O., Körner, S., Heimann, M., Dlugokencky, E. J., and Goede, A.: Satellite chartography of atmospheric methane from SCIAMACHY on board ENVISAT: 2. Evaluation based on inverse model simulations, Journal of Geophysical Research, 112, D02 304, https://doi.org/10.1029/2006JD007268, http://doi.wiley.com/10.1029/2006JD007268, 2007.

Bergamaschi, P., Frankenberg, C., Meirink, J. F., Krol, M., Villani, M. G., Houweling, S., Dentener, F., Dlugokencky, E. J., Miller, J. B., Gatti, L. V., Engel, A., and Levin, I.: Inverse modeling of global and regional CH ₄ emissions using SCIAMACHY satellite retrievals, Journal of Geophysical Research, 114, D22 301, https://doi.org/10.1029/2009JD012287, http://doi.wiley.com/10.1029/2009JD012287, 2009.

Bloom, A. A., Bowman, W. K., Lee, M., Turner, J. A., Schroeder, R., Worden, R. J., Weidner, R., McDonald, C. K., and Jacob, J. D.: A global wetland methane emissions and uncertainty dataset for atmospheric chemical transport models (WetCHARTs version 1.0), Geoscientific Model Development, 10, 2141–2156, https://doi.org/10.5194/gmd-10-2141-2017, https://doi.org/10.5194/gmd-10-2141-2017, 2017.

Botía B., S., Gerbig, C., Marshall, J., Lavric, J., Walter, D., Pöhlker, C., Holanda, B., Fisch, G., de Araujo, A. C., Sá, M., Teixeira, P., Resende, A., Dias-Junior, C., van Asperen, H., Oliveira, P., Stefanello, M., and Acevedo, O.: Understanding nighttime methane signals at the Amazon Tall Tower Observatory (ATTO), Atmospheric Chemistry and Physics Discussions, pp. 1–43, https://doi.org/10.5194/acp-2019-977, https://doi.org/10.5194/acp-2019-977, 2019.

Calvo Buendia, E., Tanabe, K., Kranjc, A., Baasansuren, J., Fukuda, M., S., N., Osako, A., Pyrozhenko, Y., Shermanau, P., and Federici, S.: 2019 Refinement to the 2006 IPCC Guidelines for National Greenhouse Gas Inventories, https://www.ipcc-nggip.iges.or.jp/public/2019rf/pdf/2019rf_all_in.zip, 2019.

Cardoso, A. d. S., Oliveira, S. C., Janusckiewicz, E. R., Brito, L. F., Morgado, E. d. S., Reis, R. A., and Ruggieri, A. C.: Seasonal effects on ammonia, nitrous oxide, and methane emissions for beef cattle excreta and urea fertilizer applied to a tropical pasture, Soil and Tillage Research, 194, 104 341, https://doi.org/10.1016/j.still.2019.104341, 2019.

Chevallier, F., Feng, L., Bösch, H., Palmer, P. I., and Rayner, P. J.: On the impact of transport model errors for the estimation of CO 2 surface fluxes from GOSAT observations, Geophysical Research Letters, 37, https://doi.org/10.1029/2010GL044652, http://www.esrl.noaa.gov/gmd/ccgg/trends/,, 2010.

Ciais, P., Sabine, C., Bala, G., Bopp, L., Brovkin, V., Canadell, J., Chhabra, A., DeFries, R., Galloway, J. M. H., Jones, C., Le Quéré, C., Myneni, R. B., Piao, S., and Thornton, P.: Working Group 1, Summary for Policymakers, in: Climate Change 2013: The Physical Science Basis. Contribution of Working Group I to the Fifth Assessment Report of the Intergovernmental Panel on Climate Change, edited by Stocker, T., Qin, D., Plattner, G.-K., Tignor, M., Allen, S., Boschung, J., Nauels, A., Xia, Y., Bex, V., and Midgley, P., Cambridge University Press, https://doi.org/10.1017/CBO9781107415324.Summary, http://www.climatechange2013.org/images/report/WG1AR5{_}SPM{_}FINAL.pdf, 2013.

Clark, D. B., Mercado, L. M., Sitch, S., Jones, C. D., Gedney, N., Best, M. J., Pryor, M., Rooney, G. G., Essery, R. L. H., Blyth, E., Boucher, O., Harding, R. J., Huntingford, C., and Cox, P. M.: The Joint UK Land Environment Simulator (JULES), model description-Part 2: Carbon fluxes and vegetation dynamics, Geoscientific Model Development, 4, 701–722, https://doi.org/10.5194/gmd-4-701-2011, www.geosci-model-dev.net/4/701/2011/, 2011.

Cunnold, D. M.: In situ measurements of atmospheric methane at GAGE/AGAGE sites during 1985–2000 and resulting source inferences, Journal of Geophysical Research, 107, 4225, https://doi.org/10.1029/2001JD001226, http://doi.wiley.com/10.1029/2001JD001226, 2002.

Dils, B., Buchwitz, M., Reuter, M., Schneising, O., Boesch, H., Parker, R., Guerlet, S., Aben, I., Blumenstock, T., Burrows, J. P., Butz, A., Deutscher, N. M., Frankenberg, C., Hase, F., Hasekamp, O. P., Heymann, J., De Mazière, M., Notholt, J., Sussmann, R., Warneke, T., Griffith, D., Sherlock, V., and Wunch, D.: The greenhouse gas climate change initiative (GHG-CCI): Comparative validation of GHG-CCI SCIAMACHY/ENVISAT and TANSO-FTS/GOSAT CO2 and CH4 retrieval algorithm products with measurements from the TCCON, Atmospheric Measurement Techniques, 7, 1723–1744, https://doi.org/10.5194/amt-7-1723-2014, 2014.

Dlugokencky, E. J., Houweling, S., Bruhwiler, L., Masarie, K. A., Lang, P. M., Miller, J. B., and Tans, P. P.: Atmospheric methane levels off: Temporary pause or a new steady-state?, Geophysical Research Letters, 30, https://doi.org/10.1029/2003GL018126, 2003.

Dlugokencky, E. J., Bruhwiler, L., White, J. W., Emmons, L. K., Novelli, P. C., Montzka, S. A., Masarie, K. A., Lang, P. M., Crotwell, A. M., Miller, J. B., and Gatti, L. V.: Observational constraints on recent increases in the atmospheric CH 4 burden, Geophysical Research Letters, 36, 3–7, https://doi.org/10.1029/2009GL039780, 2009.

Emmons, L. K., Walters, S., Hess, P. G., Lamarque, J.-F., Pfister, G. G., Fillmore, D., Granier, C., Guenther, A., Kinnison, D., Laepple, T., Orlando, J., Tie, X., Tyndall, G., Wiedinmyer, C., Baughcum, S. L., and Kloster, S.: Geoscientific Model Development Description and evaluation of the Model for Ozone and Related chemical Tracers, version 4 (MOZART-4), Geoscientific Model Development, 3, 43–67, www.geosci-model-dev.net/3/43/2010/, 2010.

Feng, L., Palmer, P. I., Yang, Y., Yantosca, R. M., Kawa, S. R., Paris, J. D., Matsueda, H., and MacHida, T.: Evaluating a 3-D transport model of atmospheric CO2 using ground-based, aircraft, and space-borne data, Atmospheric Chemistry and Physics, 11, 2789–2803, https://doi.org/10.5194/acp-11-2789-2011, 2011.

Feng, L., Palmer, P. I., Bösch, H., Parker, R. J., Webb, A. J., Correia, C. S. C., Deutscher, N. M., Domingues, L. G., Feist, D. G., Gatti, L. V., Gloor, E., Hase, F., Kivi, R., Liu, Y., Miller, J. B., Morino, I., Sussmann, R., Strong, K., Uchino, O., Wang, J., and Zahn, A.: Consistent regional fluxes of CH 4 and CO 2 inferred from GOSAT proxy XCH 4 : XCO 2 retrievals, 2010–2014, Atmospheric Chemistry and Physics, 17, 4781–4797, https://doi.org/10.5194/acp-17-4781-2017, https://www.atmos-chem-phys.net/17/4781/2017/, 2017.

Frankenberg, C., Aben, I., Bergamaschi, P., Dlugokencky, E. J., Van Hees, R., Houweling, S., Van Der Meer, P., Snel, R., and Tol, P.: Global column-averaged methane mixing ratios from 2003 to 2009 as derived from SCIAMACHY: Trends and variability, Journal of Geophysical Research Atmospheres, 116, 1–12, https://doi.org/10.1029/2010JD014849, 2011.

Ganesan, A. L., Rigby, M., Zammit-Mangion, A., Manning, A. J., Prinn, R. G., Fraser, P. J., Harth, C. M., Kim, K. R., Krummel, P. B., Li, S., Mühle, J., O'Doherty, S. J., Park, S., Salameh, P. K., Steele, L. P., and Weiss, R. F.: Characterization of uncertainties in atmospheric trace gas inversions using hierarchical Bayesian methods, Atmospheric Chemistry and Physics, 14, 3855–3864, https://doi.org/10.5194/acp-14-3855-2014, 2014.

Ganesan, A. L., Rigby, M., Lunt, M. F., Parker, R. J., Boesch, H., Goulding, N., Umezawa, T., Zahn, A., Chatterjee, A., Prinn, R. G., Tiwari, Y. K., van der Schoot, M., and Krummel, P. B.: Atmospheric observations show accurate reporting and little growth in India's methane emissions, Nature Communications, 8, 836, https://doi.org/10.1038/s41467-017-00994-7, http://www.nature.com/articles/s41467-017-00994-7, 2017.

Ganesan, A. L., Stell, A. C., Gedney, N., Comyn-Platt, E., Hayman, G., Rigby, M., Poulter, B., and Hornibrook, E. R.: Spatially Resolved Isotopic Source Signatures of Wetland Methane Emissions, Geophysical Research Letters, 45, 3737–3745, https://doi.org/10.1002/2018GL077536, 2018.

Ganesan, A. L., Schwietzke, S., Poulter, B., Arnold, T., Lan, X., Rigby, M., Vogel, F. R., van der Werf, G. R., Janssens-Maenhout, G., Boesch, H., Pandey, S., Manning, A. J., Jackson, R. B., Nisbet, E. G., and Manning, M. R.: Advancing Scientific Understanding of the Global Methane Budget in Support of the Paris Agreement, Global Biogeochemical Cycles, 33, 1475–1512, https://doi.org/10.1029/2018GB006065, https://onlinelibrary.wiley.com/doi/abs/10.1029/2018GB006065, 2019.

Gumbricht, T., Roman-Cuesta, R. M., Verchot, L., Herold, M., Wittmann, F., Householder, E., Herold, N., and Murdiyarso, D.: An expert system model for mapping tropical wetlands and peatlands reveals South America as the largest contributor, Global Change Biology, 23, 3581–3599, https://doi.org/10.1111/gcb.13689, http://doi.wiley.com/10.1111/gcb.13689, 2017.

Imbiriba, B. C. O., Ramos, J. R. d. S., de Sousa Silva, R., Cattanio, J. H., do Couto, L. L., and Mitschein, T. A.: Estimates of methane emissions and comparison with gas mass burned in CDM action in a large landfill in Eastern Amazon, Waste Management, 101, 28–34, https://doi.org/10.1016/j.wasman.2019.09.029, 2020.

Janardanan, R., Maksyutov, S., Tsuruta, A., Wang, F., Tiwari, Y. K., Valsala, V., Ito, A., Yoshida, Y., Kaiser, J. W., and Janssens-maenhout, G.: Country-Scale Analysis of Methane Emissions With a High-Resolution Inverse Model Using GOSAT and Surface Observations, Remote Sensing, 12, 1–27, https://doi.org/10.3390/rs12030375, https://www.mdpi.com/2072-4292/12/3/375, 2020.

Janssens-Maenhout, G., Crippa, M., Guizzardi, D., Muntean, M., Schaaf, E., Dentener, F., Bergamaschi, P., Pagliari, V., Olivier, J. G. J., Peters, J. A. H. W., Van Aardenne, J. A., Monni, S., Doering, U., and Petrescu, A. M. R.: EDGAR v4.3.2 Global Atlas of the three major Greenhouse Gas Emissions for the period 1970-2012, https://doi.org/10.5194/essd-2017-79, http://edgar.jrc.ec.europa.eu/overview.php?v=432{&}SECURE=123, 2017.

Jones, A., Thomson, D., Hort, M., and Devenish, B.: The U.K. Met Office's Next-Generation Atmospheric Dispersion Model, NAME III, pp. 580–589, https://doi.org/10.1007/978-0-387-68854-1_62, 2007.

Lewis, S. L., Brando, P. M., Phillips, O. L., Van Der Heijden, G. M., and Nepstad, D.: The 2010 Amazon drought, Science, 331, 554, https://doi.org/10.1126/science.1200807, 2011.

Lunt, M. F., Rigby, M., Ganesan, A. L., and Manning, A. J.: Estimation of trace gas fluxes with objectively determined basis functions using reversible-jump Markov chain Monte Carlo, Geoscientific Model Development, 9, 3213–3229, https://doi.org/10.5194/gmd-9-3213-2016, 2016.

Machado, S. L., Carvalho, M. F., Gourc, J. P., Vilar, O. M., and do Nascimento, J. C.: Methane generation in tropical landfills: Simplified methods and field results, Waste Management, 29, 153–161, https://doi.org/10.1016/j.wasman.2008.02.017, 2009.

McNorton, J., Wilson, C., Gloor, M., Parker, R. J., Boesch, H., Feng, W., Hossaini, R., and Chipperfield, M. P.: Attribution of recent increases in atmospheric methane through 3-D inverse modelling, Atmospheric Chemistry and Physics, 18, 18 149–18 168, https://doi.org/10.5194/acp-18-18149-2018, https://doi.org/10.5194/acp-18-18149-2018, 2018.

Miller, J. B., Gatti, L. V., D'Amelio, M. T., Crotwell, A. M., Dlugokencky, E. J., Bakwin, P., Artaxo, P., and Tans, P. P.: Airborne measurements indicate large methane emissions from the eastern Amazon basin, Geophysical Research Letters, 34, https://doi.org/10.1029/2006GL029213, www.cdc.noaa.gov/cdc/data.ncep., 2007.

Ministry of Foreign Affairs, Ministry of Science, T. I., and Communications: Brazil's Third Biennial Update Report to the United Nations Framework Convention on Climate Change, https://unfccc.int/sites/default/files/resource/2018-02-28{_}BRA-BUR3{_}ENG{_}FINAL.pdf, 2019.

Ministry of Science, T. and Innovation: Third National Communication of Brazil to the United Nations Framework Convention on Climate Change – Volume I, https://unfccc.int/sites/default/files/resource/branc3v1.pdf, 2016.

Monteil, G., Houweling, S., Dlugockenky, E. J., Maenhout, G., Vaughn, B. H., White, J. W., and Rockmann, T.: Interpreting methane variations in the past two decades using measurements of CH4 mixing ratio and isotopic composition, Atmospheric Chemistry and Physics, 11, 9141–9153, https://doi.org/10.5194/acp-11-9141-2011, www.atmos-chem-phys.net/11/9141/2011/, 2011.

Nguyen, N. H., Turner, A. J., Yin, Y., Prather, M. J., and Frankenberg, C.: Effects of Chemical Feedbacks on Decadal Methane Emissions Estimates, Geophysical Research Letters, 47, 1–13, https://doi.org/10.1029/2019GL085706, 2020.

Nisbet, E., Fisher, R., Lowry, D., France, J., Allen, G., Bakkaloglu, S., Broderick, T., Cain, M., Coleman, M., Fernandez, J., Forster, G., Griffiths, P., Iverach, C., Kelly, B., Manning, M., Nisbet-Jones, P., Pyle, J., Townsend-Small, A., Al-Shalaan, A., Warwick, N., and Zazzeri, G.: Methane mitigation: methods to reduce emissions, on the path to the Paris Agreement, Reviews of Geophysics, 58, https://doi.org/10.1029/2019rg000675, 2020.

Nisbet, E. G., Dlugokencky, E. J., Manning, M. R., Lowry, D., Fisher, R. E., France, J. L., Michel, S. E., Miller, J. B., White, J. W., Vaughn, B., Bousquet, P., Pyle, J. A., Warwick, N. J., Cain, M., Brownlow, R., Zazzeri, G., Lanoisellé, M., Manning, A. C., Gloor, E., Worthy, D. E., Brunke, E. G., Labuschagne, C., Wolff, E. W., and Ganesan, A. L.: Rising atmospheric methane: 2007–2014 growth and isotopic shift, Global Biogeochemical Cycles, 30, 1356–1370, https://doi.org/10.1002/2016GB005406, http://doi.wiley.com/10.1002/2016GB005406, 2016.

Nisbet, E. G., Manning, M. R., Dlugokencky, E. J., Fisher, R. E., Lowry, D., Michel, S. E., Myhre, C. L., Platt, S. M., Allen, G., Bousquet, P., Brownlow, R., Cain, M., France, J. L., Hermansen, O., Hossaini, R., Jones, A. E., Levin, I., Manning, A. C., Myhre, G., Pyle, J. A., Vaughn, B. H., Warwick, N. J., and White, J. W. C.: Very Strong Atmospheric Methane Growth in the 4 Years 2014–2017: Implications for the Paris Agreement, Global Biogeochemical Cycles, 33, 318–342, https://doi.org/10.1029/2018GB006009, https://onlinelibrary.wiley.com/doi/abs/10.1029/2018GB006009, 2019.

Oki, T., Nishimura, T., and Dirmeyer, P.: Assessment of Annual Runoff from Land Surface Models Using Total Runoff Integrating Pathways (TRIP), Journal of the Meteorological Society of Japan. Ser. II, 77, 235–255, https://doi.org/10.2151/jmsj1965.77.1B_235, 1999.

Palmer, P. I., O'Doherty, S., Allen, G., Bower, K., Bösch, H., Chipperfield, M. P., Connors, S., Dhomse, S., Feng, L., Finch, D. P., Gallagher, M. W., Gloor, E., Gonzi, S., Harris, N. R., Helfter, C., Humpage, N., Kerridge, B., Knappett, D., Jones, R. L., Le Breton, M., Lunt, M. F., Manning, A. J., Matthiesen, S., Muller, J. B., Mullinger, N., Nemitz, E., O'Shea, S., Parker, R. J., Percival, C. J., Pitt, J., Riddick, S. N., Rigby, M., Sembhi, H., Siddans, R., Skelton, R. L., Smith, P., Sonderfeld, H., Stanley, K., Stavert, A. R., Wenger, A., White, E., Wilson, C.,

and Young, D.: A measurement-based verification framework for UK greenhouse gas emissions: An overview of the Greenhouse gAs Uk and Global Emissions (GAUGE) project, Atmospheric Chemistry and Physics, 18, 11 753–11 777, https://doi.org/10.5194/acp-18-11753-2018, https://www.atmos-chem-phys.net/18/11753/2018/, 2018.

Pangala, S. R., Enrich-Prast, A., Basso, L. S., Peixoto, R. B., Bastviken, D., Hornibrook, E. R. C., Gatti, L. V., Ribeiro, H., Calazans, L. S. B., Sakuragui, C. M., Bastos, W. R., Malm, O., Gloor, E., Miller, J. B., and Gauci, V.: Large emissions from floodplain trees close the Amazon methane budget, Nature, 552, 230, https://doi.org/10.1038/nature24639, http://www.nature.com/doifinder/10.1038/nature24639, 2017.

Parker, R., Boesch, H., Cogan, A., Fraser, A., Feng, L., Palmer, P. I., Messerschmidt, J., Deutscher, N., Griffith, D. W. T., Notholt, J., Wennberg, P. O., and Wunch, D.: Methane observations from the Greenhouse Gases Observing SATellite: Comparison to ground-based TCCON data and model calculations, Geophysical Research Letters, 38, 2–7, https://doi.org/10.1029/2011GL047871, 2011.

Parker, R. J., Boesch, H., Byckling, K., Webb, A. J., Palmer, P. I., Feng, L., Bergamaschi, P., Chevallier, F., Notholt, J., Deutscher, N., Warneke, T., Hase, F., Sussmann, R., Kawakami, S., Kivi, R., Griffith, D. W., and Velazco, V.: Assessing 5 years of GOSAT Proxy XCH4 data and associated uncertainties, Atmospheric Measurement Techniques, 8, 4785–4801, https://doi.org/10.5194/amt-8-4785-2015, 2015.

Parker, R. J., Boesch, H., McNorton, J., Comyn-Platt, E., Gloor, M., Wilson, C., Chipperfield, M. P., Hayman, G. D., and Bloom, A. A.: Evaluating year-to-year anomalies in tropical wetland methane emissions using satellite CH4observations, Remote Sensing of Environment, 211, 261–275, https://doi.org/10.1016/j.rse.2018.02.011, 2018.

Peters, W., Jacobson, A. R., Sweeney, C., Andrews, A. E., Conway, T. J., Masarie, K., Miller, J. B., Bruhwiler, L. M., Pétron, G., Hirsch, A. I., Worthy, D. E., Van Der Werf, G. R., Randerson, J. T., Wennberg, P. O., Krol, M. C., and Tans, P. P.: An atmospheric perspective on North American carbon dioxide exchange: CarbonTracker, Proceedings of the National Academy of Sciences of the United States of America, 104, 18 925–18 930, https://doi.org/10.1073/pnas.0708986104, 2007.

Pisso, I., Sollum, E., Grythe, H., Kristiansen, N. I., Cassiani, M., Eckhardt, S., Arnold, D., Morton, D., Thompson, R. L., Groot Zwaaftink, C. D., Evangeliou, N., Sodemann, H., Haimberger, L., Henne, S., Brunner, D., Burkhart, J. F., Fouilloux, A., Brioude, J., Philipp, A., Seibert, P., and Stohl, A.: The Lagrangian particle dispersion model FLEXPART version 10.4, Geoscientific Model Development, 12, 4955–4997, https://doi.org/10.5194/gmd-12-4955-2019, 2019.

Pöhlker, C., Walter, D., Paulsen, H., Könemann, T., Rodríguez-Caballero, E., Moran-Zuloaga, D., Brito, J., Carbone, S., Degrendele, C., Després, V. R., Ditas, F., Holanda, B. A., Kaiser, J. W., Lammel, G., Lavrič, J. V., Ming, J., Pickersgill, D., Pöhlker, M. L., Praß, M., Löbs, N., Saturno, J., Sörgel, M., Wang, Q., Weber, B., Wolff, S., Artaxo, P., Pöschl, U., and Andreae, M. O.: Land cover and its transformation in the backward trajectory footprint region of the Amazon Tall Tower Observatory, Atmospheric Chemistry and Physics, 19, 8425–8470, https://doi.org/10.5194/acp-19-8425-2019, 2019.

Prinn, R. G., Weiss, R. F., Arduini, J., Arnold, T., DeWitt, H. L., Fraser, P. J., Ganesan, A. L., Gasore, J., Harth, C. M., Hermansen, O., Kim, J., Krummel, P. B., Li, S., Loh, Z. M., Lunder, C. R., Maione, M., Manning, A. J., Miller, B. R., Mitrevski, B., Mühle, J., O'Doherty, S., Park, S., Reimann, S., Rigby, M., Saito, T., Salameh, P. K., Schmidt, R., Simmonds, P. G., Steele, L. P., Vollmer, M. K., Wang, R. H., Yao, B., Yokouchi, Y., Young, D., and Zhou, L.: History of chemically and radiatively important atmospheric gases from the Advanced Global Atmospheric Gases Experiment (AGAGE), Earth System Science Data, 10, 985–1018, https://doi.org/10.5194/essd-10-985-2018, https://www.earth-syst-sci-data.net/10/985/2018/, 2018.

Rigby, M., Prinn, R. G., Fraser, P. J., Simmonds, P. G., Langenfelds, R. L., Huang, J., Cunnold, D. M., Steele, L. P., Krummel, P. B., Weiss, R. F., O'Doherty, S., Salameh, P. K., Wang, H. J., Harth, C. M., Mühle, J., and Porter, L. W.: Renewed growth of atmospheric methane, Geophysical Research Letters, 35, 2–7, https://doi.org/10.1029/2008GL036037, 2008.

Rigby, M., Montzka, S. A., Prinn, R. G., White, J. W. C., Young, D., O'Doherty, S., Lunt, M. F., Ganesan, A. L., Manning, A. J., Simmonds, P. G., Salameh, P. K., Harth, C. M., Mühle, J., Weiss, R. F., Fraser, P. J., Steele, L. P., Krummel, P. B., McCulloch, A., and Park, S.: Role of atmospheric oxidation in recent methane growth, Proceedings of the National Academy of Sciences, 114, 5373–5377, https://doi.org/10.1073/pnas.1616426114, http://www.pnas.org/lookup/doi/10.1073/pnas.1616426114, 2017.

Saunois, M., Bousquet, P., Poulter, B., Peregon, A., Ciais, P., Canadell, J. G., Dlugokencky, E. J., Etiope, G., Bastviken, D., Houweling, S., Janssens-Maenhout, G., Tubiello, F. N., Castaldi, S., Jackson, R. B., Alexe, M., Arora, V. K., Beerling, D. J., Bergamaschi, P., Blake, D. R., Brailsford, G., Brovkin, V., Bruhwiler, L., Crevoisier, C., Crill, P., Covey, K., Curry, C., Frankenberg, C., Gedney, N., Höglund-Isaksson, L., Ishizawa, M., Ito, A., Joos, F., Kim, H. S., Kleinen, T., Krummel, P., Lamarque, J. F., Langenfelds, R., Locatelli, R., Machida, T., Maksyutov, S., McDonald, K. C., Marshall, J., Melton, J. R., Morino, I., Naik, V., O'Doherty, S., Parmentier, F. J. W., Patra, P. K., Peng, C., Peng, S., Peters, G. P., Pison, I., Prigent, C., Prinn, R., Ramonet, M., Riley, W. J., Saito, M., Santini, M., Schroeder, R., Simpson, I. J., Spahni, R., Steele, P., Takizawa, A., Thornton, B. F., Tian, H., Tohjima, Y., Viovy, N., Voulgarakis, A., Van Weele, M., Van Der Werf, G. R., Weiss, R., Wiedinmyer, C., Wilton, D. J., Wiltshire, A., Worthy, D., Wunch, D., Xu, X., Yoshida, Y., Zhang, B., Zhang, Z., and Zhu, Q.: The global methane budget 2000-2012, Earth System Science Data, 8, 697–751, https://doi.org/10.5194/essd-8-697-2016, 2016.

Schaefer, H., Fletcher, S. E., Veidt, C., Lassey, K. R., Brailsford, G. W., Bromley, T. M., Dlugokencky, E. J., Michel, S. E., Miller, J. B., Levin, I., Lowe, D. C., Martin, R. J., Vaughn, B. H., and White, J. W.: A 21st-century shift from fossil-fuel to biogenic methane emissions indicated by 13CH4, https://doi.org/10.1126/science.aad2705, https://science.sciencemag.org/content/352/6281/80, 2016.

Schroeder, R., McDonald, K. C., Chapman, B. D., Jensen, K., Podest, E., Tessler, Z. D., Bohn, T. J., and Zimmermann, R.: Development and evaluation of a multi-year fractional surface water data set derived from active/passive microwave remote sensing data, Remote Sensing, 7, 16 688–16 732, https://doi.org/10.3390/rs71215843, http://www.mdpi.com/2072-4292/7/12/15843, 2015.

Schulz, C., Whitney, B. S., Rossetto, O. C., Neves, D. M., Crabb, L., de Oliveira, E. C., Terra Lima, P. L., Afzal, M., Laing, A. F., de Souza Fernandes, L. C., da Silva, C. A., Steinke, V. A., Torres Steinke, E., and Saito, C. H.: Physical, ecological and human dimensions of environmental change in Brazil's Pantanal wetland: Synthesis and research agenda, 687, 1011–1027, https://doi.org/10.1016/j.scitotenv.2019.06.023, 2019.

Schwietzke, S., Sherwood, O. A., Bruhwiler, L. M., Miller, J. B., Etiope, G., Dlugokencky, E. J., Michel, S. E., Arling, V. A., Vaughn, B. H., White, J. W., and Tans, P. P.: Upward revision of global fossil fuel methane emissions based on isotope database, Nature, 538, 88–91, https://doi.org/10.1038/nature19797, http://www.nature.com/doifinder/10.1038/nature19797, 2016.

Turner, A. J., Jacob, D. J., Wecht, K. J., Maasakkers, J. D., Lundgren, E., Andrews, A. E., Biraud, S. C., Boesch, H., Bowman, K. W., Deutscher, N. M., Dubey, M. K., Griffith, D. W., Hase, F., Kuze, A., Notholt, J., Ohyama, H., Parker, R., Payne, V. H., Sussmann, R., Sweeney, C., Velazco, V. A., Warneke, T., Wennberg, P. O., and Wunch, D.: Estimating global and North American methane emissions with high spatial resolution using GOSAT satellite data, Atmospheric Chemistry and Physics, 15, 7049–7069, https://doi.org/10.5194/acp-15-7049-2015, www.atmos-chem-phys.net/15/7049/2015/, 2015.

Turner, A. J., Frankenberg, C., Wennberg, P. O., and Jacob, D. J.: Ambiguity in the causes for decadal trends in atmospheric methane and hydroxyl., Proceedings of the National Academy of Sciences of the United States of America, 114, 5367–5372, https://doi.org/10.1073/pnas.1616020114, http://www.ncbi.nlm.nih.gov/pubmed/28416668http://www.pubmedcentral.nih.gov/articlerender.fcgi?artid=PMC5448216, 2017.

Turner, A. J., Frankenberg, C., and Kort, E. A.: Interpreting contemporary trends in atmospheric methane, 116, 2805–2813, https://doi.org/10.1073/pnas.1814297116, www.pnas.org/cgi/doi/10.1073/pnas.1814297116, 2019.

UNFCCC: United Nations Framework Convention on Climate Change Paris Agreement, https://unfccc.int/process-and-meetings/the-paris-agreement/the-paris-agreement, 2015.

van der Laan-Luijkx, I. R., Krol, M. C., Gatti, L. V., Domingues, L. G., Correia, C. S. C., Miller, J. B., Gloor, M., Leeuwen, T. T., Kaiser, J. W., Wiedinmyer, C., Basu, S., Clerbaux, C., and Peters, W.: Global Biogeochemical Cycles drought derived with CarbonTracker South America, Global Biogeochemical Cycles, 29, 1092–1108, https://doi.org/10.1002/2014GB005082.Received, 2015.

Van Der Werf, G. R., Randerson, J. T., Giglio, L., Van Leeuwen, T. T., Chen, Y., Rogers, B. M., Mu, M., Van Marle, M. J., Morton, D. C., Collatz, G. J., Yokelson, R. J., and Kasibhatla, P. S.: Global fire emissions estimates during 1997-2016, Earth System Science Data, 9, 697–720, https://doi.org/10.5194/essd-9-697-2017, http://www.globalfiredata.org., 2017.

Webb, A. J., Bösch, H., Parker, R. J., Gatti, L. V., Gloor, E., Palmer, P. I., Basso, L. S., Chipperfield, M. P., Correia, C. S., Domingues, L. G., Feng, L., Gonzi, S., Miller, J. B., Warneke, T., and Wilson, C.: CH4 concentrations over the Amazon from GOSAT consistent with in situ vertical profile data, Journal of Geophysical Research, 121, 11,006–11,020, https://doi.org/10.1002/2016JD025263, https://www.research.ed.ac.uk/portal/files/29145490/29145443.{_}PFV.{_}Webb{_}et{_}al{_}2016{_}Journal{_}of{_}Geophysical{_}Research{_}Atmospheres.pdf, 2016.

Wilson, C., Gloor, M., Gatti, L. V., Miller, J. B., Monks, S. A., McNorton, J., Bloom, A. A., Basso, L. S., and Chipperfield, M. P.: Contribution of regional sources to atmospheric methane over the Amazon Basin in 2010 and 2011, Global Biogeochemical Cycles, 30, 400–420, https://doi.org/10.1002/2015GB005300, 2016.

Worden, J. R., Bloom, A. A., Pandey, S., Jiang, Z., Worden, H. M., Walker, T. W., Houweling, S., and Röckmann, T.: Reduced biomass burning emissions reconcile conflicting estimates of the post-2006 atmospheric methane budget, Nature Communications, 8, 2227, https://doi.org/10.1038/s41467-017-02246-0, http://www.nature.com/articles/s41467-017-02246-0, 2017.

Wunch, D., Toon, G. C., Blavier, J. F. L., Washenfelder, R. A., Notholt, J., Connor, B. J., Griffith, D. W., Sherlock, V., and Wennberg, P. O.: The total carbon column observing network, Philosophical Transactions of the Royal Society A: Mathematical, Physical and Engineering Sciences, 369, 2087–2112, https://doi.org/10.1098/rsta.2010.0240, 2011.

Zhang, Z., Zimmermann, N. E., Calle, L., Hurtt, G., Chatterjee, A., and Poulter, B.: Enhanced response of global wetland methane emissions to the 2015-2016 El Niño-Southern Oscillation event, Environmental Research Letters, 13, https://doi.org/10.1088/1748-9326/aac939, 2018.